AD-A155 210 MAGNETIC EFFECTS IN NON-CRYSTALLINE SEMICONDUCTORS(U) 1/2
UTAH UNIV SALT LAKE CITY DEPT OF PHYSICS P C TAYLOR
1983 N00014-83-K-0535

UNCLASSIFIED F/G 20/12 NL

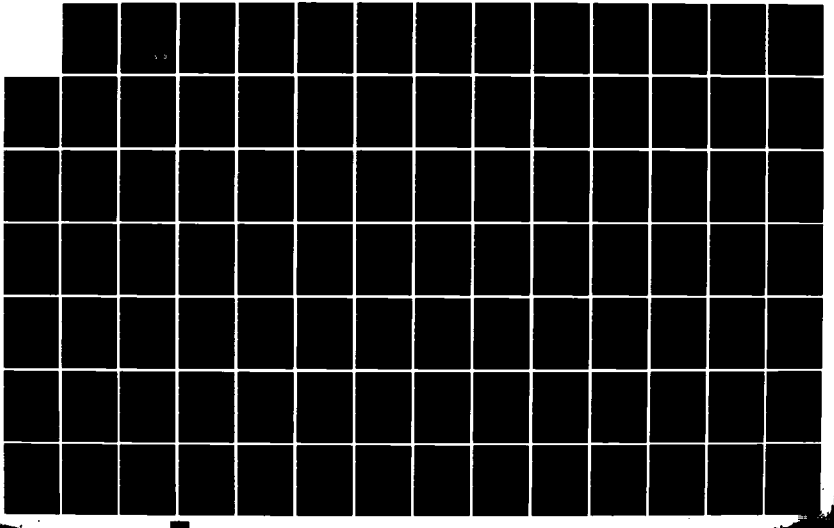

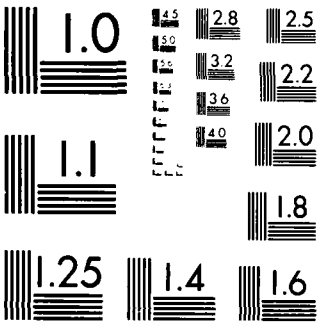

MICROCOPY RESOLUTION TEST CHART
NATIONAL BUREAU OF STANDARDS-1963-A

83-K-0535-2

MAGNETIC EFFECTS IN NON-CRYSTALLINE SEMICONDUCTORS

P. Craig Taylor
Department of Physics
University of Utah
Salt Lake City, UT 84112

85 5 20 002

SECURITY CLASSIFICATION OF THIS PAGE (When Data Entered)

REPORT DOCUMENTATION PAGE

READ INSTRUCTIONS BEFORE COMPLETING FORM

1. REPORT NUMBER: 83-K-0535-2
2. GOVT ACCESSION NO.:
3. RECIPIENT'S CATALOG NUMBER:

4. TITLE (and Subtitle): MAGNETIC EFFECTS IN NON-CRYSTALLINE SEMICONDUCTORS
5. TYPE OF REPORT & PERIOD COVERED: Interim
6. PERFORMING ORG. REPORT NUMBER:

7. AUTHOR(s): P.C. Taylor
8. CONTRACT OR GRANT NUMBER(s): N00014-83-K-0535

9. PERFORMING ORGANIZATION NAME AND ADDRESS:
University of Utah
Physics Department
Salt Lake City, UT 84112

10. PROGRAM ELEMENT, PROJECT, TASK AREA & WORK UNIT NUMBERS: 372-152

11. CONTROLLING OFFICE NAME AND ADDRESS:
Office of Naval Research
800 N. Quincy St.
Atlington, VA 22217

12. REPORT DATE:
13. NUMBER OF PAGES:

14. MONITORING AGENCY NAME & ADDRESS (if different from Controlling Office): Same as above

15. SECURITY CLASS. (of this report): Unclassified
15a. DECLASSIFICATION/DOWNGRADING SCHEDULE:

16. DISTRIBUTION STATEMENT (of this Report): Unlimited

17. DISTRIBUTION STATEMENT (of the abstract entered in Block 20, if different from Report): Same as above

18. SUPPLEMENTARY NOTES:

19. KEY WORDS (Continue on reverse side if necessary and identify by block number): NMR, ESR, NQR, Magnetic Resonance, Non-Crystalline Semiconductors, Amorphous Semiconductors

20. ABSTRACT (Continue on reverse side if necessary and identify by block number)

(See next page.)

DD FORM 1473 EDITION OF 1 NOV 65 IS OBSOLETE
S/N 0102-LF-014-6601

SECURITY CLASSIFICATION OF THIS PAGE (When Data Entered)

20. Abstract

Most amorphous semiconductors are essentially diamagnetic, but a paramagnetic contribution to the magnetic susceptibility is present in some materials due to either the presence of inadvertent paramagnetic impurities or the existence of paramagnetic defects such as unsatisfied or dangling bonds. When light of energy near the band gap energy is applied to these semiconductors there is an optically-induced paramagnetism which results. In most cases this optically-induced paramagnetism is metastable at low enough temperatures. Although the exact cause of the paramagnetism depends on the specific amorphous semiconductor, two general mechanisms have been identified: the optical rearrangement of charge in existing defects or the optically-induced creation of new defects. In either of these cases the optically-induced paramagnetism can be annealed, in some cases optically and in all cases by heating well below the glass transition or crystallization temperatures.

Magnetic effects can be used effectively to probe local structural order of defects, impurities or major constituent atoms. Some magnetic processes are also useful in probing low energy excitations in amorphous semiconductors. The primary techniques are electron spin resonance (ESR), nuclear magnetic resonance (NMR), nuclear quadrupole resonance (NQR) and Mössbauer spectroscopy. Optical techniques coupled with magnetic resonance can also yield important information concerning absorption and recombination processes in amorphous semiconductors. Such a technique is optically detected magnetic resonance (ODMR) where changes in absorption or photoluminescence (PL) processes are monitored as the sample goes through an ESR or NMR process.

I. INTRODUCTION

Most amorphous semiconductors are essentially diamagnetic, but a paramagnetic contribution to the magnetic susceptibility is present in some materials due to either the presence of inadvertent paramagnetic impurities or the existence of paramagnetic defects such as unsatisfied or dangling bonds. When light of energy near the band gap energy is applied to these semiconductors there is an optically-induced paramagnetism which results. In most cases this optically-induced paramagnetism is metastable at low enough temperatures. Although the exact cause of the paramagnetism depends on the specific amorphous semiconductor, two general mechanisms have been identified: the optical rearrangement of charge in existing defects or the optically-induced creation of new defects. In either of these cases the optically-induced paramagnetism can be annealed, in some cases optically and in all cases by heating well below the glass transition or crystallization temperatures.

Magnetic effects can be used effectively to probe local structural order of defects, impurities or major constituent atoms. Some magnetic processes are also useful in probing low energy excitations in amorphous semiconductors. The primary techniques are electron spin resonance (ESR), nuclear magnetic resonance (NMR), nuclear quadrupole resonance (NQR) and Mössbauer spectroscopy. Optical techniques coupled with magnetic resonance can also yield important information concerning absorption and recombination processes in amorphous semiconductors. Such a technique is optically detected magnetic resonance (ODMR) where changes in absorption or photoluminescence (PL) processes are monitored as the sample goes through an ESR or NMR process.

In section II the normal diamagnetic behavior of amorphous semiconductors is discussed. Section III considers paramagnetic effects such as those due to native defects or impurities or to optically-induced changes in the material.

This section also summarizes the important relaxation mechanisms for electronic spins via the atoms in the lattice (spin-lattice relaxation). In Section IV the important results of NMR and NQR measurements in amorphous semiconductors are discussed. These results include the use of NMR and NQR as probes of local bonding arrangements and the use of nuclear spin-lattice relaxation to probe low energy vibrational excitations or impurity species in amorphous semiconductors. Sections V and VI briefly summarize the most important applications of Mössbauer and ODMR spectroscopy, to amorphous semiconductors. Significant conclusions are summarized in section VII.

II. DIAMAGNETISM

With the exception of some tetrahedrally bonded amorphous semiconductors to be discussed in Section III.A.2, most amorphous semiconductors are diamagnetic under equilibrium conditions. The magnetic susceptibility χ in amorphous semiconductors is often more diamagnetic than the average susceptibility of the corresponding crystalline modifications,[1] although this so-called "diamagnetic enhancement" is not as strong or as universal as originally thought.[2-5]

Early experiments on glassy Se,[6] or $CdGe_xAs_2$ and related glasses,[7-9] and on As_2S_3 and As_2Se_3 glasses[3,4,10] yielded enhancements in the diamagnetic susceptibility of over 50% between the glassy and crystalline phases. More careful experiments have subsequently confirmed that these enhancements are much less than originally thought. For example, in S and Se there is no enhancement within experimental error[11] as is shown in Table 1. Similarly, in glassy As_2S_3 and As_2Se_3 there is at most an enhancement of ~ 3% which is also within experimental error.[1]

In Fig. 1 are presented data of Di Salvo et al.[1] for the magnetic susceptibility in pure samples of glassy As_2S_3 and As_2Se_3. As can be seen from

the figure, both glasses exhibit a temperature independent, diamagnetic susceptibility which dominates down to at least 10 K. Below 10 K there is a paramagnetic contribution to the susceptibility which is due to impurities.

In tetrahedrally bonded amorphous semiconductors the increase in diamagnetism in the amorphous phase can be slightly greater[8] (~ 4% in $CdAs_2$; see Table 1), but these materials are difficult to prepare and contain a paramagnetic contribution to the susceptibility due to unsatisfied bonds. These materials are poor glass formers and must be rapidly quenched from the melt in small volumes in order to obtain the amorphous phase.

Comparisons with crystalline solids must, of course, be made with some care. Because most crystalline counterparts are anisotropic, comparisons of the isotropic glassy phase must be made with a suitable average of the susceptibilities in the principal crystalline directions.[1] In addition, there are often several crystalline polymorphs which compositionally match a given glass, as for example, the trigonal and monoclinic forms of selenium.

To the extent that there is an enhancement of the diamagnetic susceptibility in glasses over their crystalline counterparts, the explanation probably arises from two mechanisms.[5] The frist mechanism is an increase in the diamagnetism associated with the large orbits of localized states. The second mechanism is a decrease in the Van Vleck paramagnetism due to interband contributions. White and Anderson[5] suggest that the second mechanism is perhaps the dominant one.

III. PARAMAGNETISM AND ESR

The chalcogenide amorphous semiconductors exhibit an enhanced diamagnetism, but there is no paramagnetic contribution to the susceptibility except after optical excitation. The most effective energies for the exciting light are

those near the band-gap energies, and the temperatures at which the optically-induced paramagnetism is metastable are typically below approximately 100 K.

The pnictide and tetrahedral amorphous semiconductors, on the other hand, typically exhibit paramagnetic behavior in the absence of any optical excitation. In amorphous silicon (a-Si) the "dark ESR" intensity is typically $n_s \approx 10^{18}$-10^{19} spins/cm^3 while in the best hydrogenated material (a-Si:H) this spin signal can be as low as 10^{15} spins/cm^3. Under optical excitation with band gap light a-Si:H also shows increases in the ESR intensity which are both transient and metastable. Unlike the chalcogenides the metastable effects are present up to approximately 400 K.

In amorphous semiconductors measurements of ESR are capable of yielding detailed local pictures of the wave functions of the unpaired spins. This information provides a probe of the bonding at such paramagnetic sites as defects, impurities or localized electronic states at the band edges ("band tail" states). The three most important terms in the spin Hamiltonian for most ESR situations in amorphous semiconductors are the electronic Zeeman, the electronic-nuclear hyperfine and the fine structure interactions. Normally the effects of spin-orbit coupling are subsumed into the Zeeman term such that the interaction can be written in parameterized form as

$$H_{ez} = \beta \vec{S} \cdot \bar{\bar{g}} \cdot \vec{H} \qquad (1)$$

where $\beta = eh/2mc$ is the Bohr magneton, $\vec{S}$ is the electronic spin operator, $\bar{\bar{g}}$ is the gyromagnetic or g-tensor and $\vec{H}$ is the externally applied magnetic field.

If the electronic state is localized to such an extent that tight binding calculations are applicable, then one may express the g-tensor in the following fashion

$$g = g_e + 2\lambda \sum_n \frac{\langle 0|L_i|n\rangle\langle n|L_i|0\rangle}{\varepsilon_0 - \varepsilon_n} \qquad (2)$$

where $g_e = 2.00229$ is the free electron g-value, λ is the spin-orbit coupling constant (an atomic parameter), and $|0\rangle$, $|n\rangle$ represent the ground and excited states for the electronic wave function, respectively. The i^{th} component of the orbital angular momentum operator L_i admixes excited states $|n\rangle$ of energy ε_n into the ground state wave function $|0\rangle$ of energy ε_0.

The hyperfine interaction, which is the second important term in the spin-Hamiltonian, couples the electronic spin to surrounding nuclear spins. This interaction can be expressed in parameterized form as

$$H_{hf} = \vec{S} \cdot \overleftrightarrow{A} \cdot \vec{I} \qquad (3)$$

where $\overleftrightarrow{A}$ is the hyperfine term and $\vec{I}$ is the nuclear spin operator. Because the components of $\overleftrightarrow{A}$ depend both on atomic parameters and on the wavefunction for the unpaired spin, the hyperfine interaction can provide detailed information concerning the local bonding at a defect or impurity site especially in the tight-binding limit.

The fine structure interaction, which is often a third important term in the spin-Hamiltonian, reflects the effect of the electric fields generated by electrons in the solid. These electric fields depend dramatically on the elements which compose the solid and on the local symmetry. In parameterized form the fine structure term can be written as

$$H_f = \vec{S} \cdot \overleftrightarrow{D} \cdot \vec{S} \qquad (4)$$

where $\overleftrightarrow{D}$ is the fine structure tensor and $\vec{S}$, the electronic spin operator, is greater than 1/2. Examples of situations where this term is important are paramagnetic rare earth or transition metal ions in which inner shell valence

electrons tend to align parallel and some other relatively infrequent situations such as triplet states for excitons or molecules.

Because the interactions in Eqs. (1), (3) and (4) involve tensors, the spin-Hamiltonian depends in general on the orientation of the paramagnetic site with respect to the experimental geometry. In particular, it can be seen from Eq. (1) that the ESR spectrum from a single crystal will depend on the orientation of the crystal with respect to the externally applied magnetic field $\vec{H}$. In polycrystalline or non-crystalline samples the individual paramagnetic, or nuclear, sites are randomly oriented with respect to the field, and the resulting ESR (or NMR) spectrum is an average over these sites which is called a "powder pattern."[12] In non-crystalline semiconductors there is often an additional average which must be performed because not all sites are identical due to distortions which vary from location to location. This latter complication means that the parameters used in the spin-Hamiltonian (Eqs. (1), (3) and (4)) do not possess unique values for all sites in the solid.

A. Paramagnetic Susceptibility

Early models of the electronic states in amorphous semicondcutors[13,14] suggested that there should be a paramagnetic contribution to the magnetic susceptibility from localized electronic states deep in the gap. In these models tails of localized single-electron states were supposed to extend so far into the gap from both the valence and conduction bands that they actually overlapped near mid-gap where they pinned the Fermi energy. These states have never been observed experimentally. In the chalcogenide semiconductors no paramagnetism is observed which is not attributable to impurities. In most tetrehedrally bonded amorphous semiconductors a paramagnetism associated with a specific bonding defect (dangling bond) is observed.

The lack of single-electron tail states extending well into the gap was first explained by Anderson[15] who suggested that localized electronic states which are intrinsic to amorphous solids do in fact exist within the gap, but that these states are always paired (doubly occupied or empty) in the ground state configuration due to an effective electronic correlation energy which is negative. In this model these states were considered to be an intrinsic property of amorphous solids (both semiconductors and insulators) and not due to specific defects or impurities. Since this original suggestion a specific model has been proposed for the chalcogenide glasses which postulates the existence of specific, well-defined, localized, diamagnetic defects whose ground state energies lie within the gap.[16-18]

1. Chalcogenide Glasses

Although there is no evidence for a paramagnetic contribution χ which is intrinsic to the amorphous phase, there is substantial evidence for such a contribution due to inadvertant impurities,[1,19] even in the purest samples. In most samples[1,19] the dominant contribution is from Fe which exists predominantly as non-magnetic Fe^{2+} and only secondarily as Fe^{3+}.

Because the amount of Fe^{3+} which typically exists in the purest of these chalcogenide glasses is small ($n_s \sim 10^{16}$ spins/cm^3), one must either perform very precise susceptibility experiments[1] down to $\sim$ 1K or extend the experiments into the millikelvin range[19] in order to observe the effect. An example of the latter approach is given in Fig. 2 for glassy As_2Se_3. In this figure the open circles represent the Curie term in χ due to $\sim$ 10 ppm of Fe doped into As_2Se_3 of which $\sim$ 1 ppm is in the Fe^{3+} valence state. From the data for pure As_2Se_3 an upper bound of $\lesssim 10^{17}$ spins/cm^3 can be placed on the paramagnetic spin density (S = 1/2, g = 2.0). A similar upper bound of $\lesssim 3 \times 10^{16}$ spins/cm^3

(S = 1/2, g = 2.0) can be placed on any paramagnetic contribution to χ from the data of Fig. 1.

Thus if there is an intrinsic contribution to the paramagnetic susceptibility in the chalcogenide glasses, it is small. ESR measurements which may not see all of the spins for technical reasons, place the upper bound for the intrinsic contribution at an even lower value.[20,21] One may safely conclude that the temperature dependent Curie magnetic susceptibility commonly observed in the chalcogenide glasses is an impurity effect predominantly due to Fe^{3+}.

2. Tetrahedral Amorphous Semiconductors

In amorphous silicon (a-Si), silicon germanium alloys (a-Si_xGe_{1-x}) and hydrogenated amorphous silicon (a-Si:H) several experiments suggest that the magnetic susceptibility follows a Curie-Weiss behavior $(\chi = C/T - \theta)$. The microscopic origin of this susceptibility is thought to be due to the presence of dangling Si or Ge bonds (see Section III.C). The magnitude of the ordering parameter θ varies considerably from experiment to experiment. Estimates range from 40-135K in a-Si_xGe_{1-x} alloys[22] to < 1K in a-Si evaporated in an ultra-high vacuum.[23] In several other experiments on a-Si:H the values of θ fall in between these two extremes.[24-26] Some studies suggest that θ is independent of the spin density n_s even for changes of n_s over several orders of magnitude.[26] In addition, there exist both surface and bulk effects in some samples.[27,28]

The magnitude of θ can be taken as a rough measure of the degree of clustering of the spins in the materials. From this statement it is apparent that clustering varies considerably from sample to sample. Most of this variation is the result of different sample preparation procedures, but the possibility that impurities play an indirect role cannot be ruled out.

The amorphous materials based on silicon and germanium can only be made in thin film form, but there is at least a class of tetrahedrally bonded amorphous semiconductors which can be made in bulk form. These glasses are various compositions of the form $Cd_xGe_{1-x}As_2$. In this glass system preliminary experiments indicated a substantial contribution ($\sim 10^{19}$ spins/cm^3) to the paramagnetic susceptibility which was attributed to Ge dangling bonds.[7,8] However, as in the chalcogenide glasses, recent measurements indicate that this term, if present at all, corresponds to a spin density[29] (S = 1/2, g = 2.0) of $n_s \lesssim 10^{17}$ spins/cm^3.

B. Impurities

As mentioned in the previous section, inadvertent impurities often play a role in the paramagnetic susceptibility of amorphous semiconductors even in the purest samples. In addition, paramagnetic impurities and as Fe^{3+} or Mn^{2+} are sometimes deliberately introduced into amorphous semiconductors to provide probes of the local structural order. Also diamagnetic impurities such as oxygen or nitorgen can form defects for which one of the charge states is paramagnetic.

1. Chalcogenide Glasses

Transition metals are often incorporated into the chalcogenide glasses in paramagnetic configurations. For example, ESR studies of many different chalcogenide glasses at temperatures between 4 and 300K have detected the presence of iron as on unintentional impurity even in the purest glasses vailable.[30,31] Only iron in the 3+ valence state (d^5 configuration) is etected via a characteristics ESR signal whose major feature is near g = 4.2. representative spectrum is shown in Fig. 3. The shape of these spectra is essentially independent of the host glass.

The strength of the Fe^{3+} resonance in As_2Se_3 is enhanced by the addition of a broad range of metallic impurities.[31] including Tl, Cu, B, Ag and In. As

two optically-induced centers are shown in Fig. 15. The wave function of one center, P_1 (Fig. 15b), is probably localized on a single phosphorus atom and may be identical to centers which exist before optical excitation (thermally-generated ESR). The second center, P_2 (Fig. 15a) is characterized by a wave function which is localized on two equivalent phosphorus atoms. The solid lines in Fig. 15 represent computer simulations assuming p-type wave functions localized on one (P_1) or two (P_2) phosphorus atoms. The relative intensities of P_1 and P_2 depend upon the excitation source (x-irradiation or optical excitation). The metastable P_2 densities decrease rapidly above 80K while those of P_1 decrease more slowly with temperature. Both P_1 and P_2 can be optically bleached with below-band-gap light.

The optically-induced signal in amorphous As is probably the analog of the P_2 center, but the resolution in the spectrum is insufficient to be certain. Whether or not there is an optically-induced analog of the P_1 phosphorus center in amorphous arsenic remains to be determined.

The existence after optical excitation of paramagnetic sites in the chalcogenide and pnictide amorphous solids is explained by several defect models[17,18,96,97] which invoke negative effective electron-electron correlation energies to explain the diamagnetic ground state. These models describe paramagnetic states localized essentially on a single chalcogenide or pnictide atom. The presence of optically-induced spins which are localized predominantly on p-orbitals of two essentialy equivalent As or P atoms (P_2) is unexpected in the context of these defect models.

3. Tetrahedral Amorphous Semiconductors

As in the case of the chalcogenide and pnictide amorphous semiconductors, optical excitation with light near or above the band gap creates several ESR signals in the tetrahedral amorphous semiconductors.[28,98,99] In contrast to

chalcogenide glasses discussed in the previous section. As in the chalcogenide glasses, these states also can be optically bleached with light of less than band gap energies ($E_g/2 \lesssim h\nu \lesssim E_g$). The density of these states, which is $\sim 10^{17}$ cm^{-3} at 4.2K, decreases continuously with increasing temperature in a similar manner to the behavior in As_2Se_3 and decreases by at least a factor of two by 100K. An analysis[92] of the observed lineshape has suggested that these states are unpaired spins localized predomimantly on As p-orbitals ($\sim$ 95%) extending over less than about three As atoms. This conclusion results from a consideration of the hyperfine interaction (Eq. (2)) and the different magnitudes of the contributions to this interaction from s and p atomic orbitals.

The thermally generated ESR response (solid line in Fig. 14) occurs in the absence of any optical excitation on a time scale which cannot be measured but is at least as fast as that required to achieve thermal equilibrium (typically a few minutes). The density of these states increase with temperature. As can be seen from Fig. 13 the lineshapes of the two responses appear to be similar, but the two signals are distinct and separable.

The general shape of the thermally generated line suggests that this paramagnetic state is also predominantly p-like ($\sim$ 95%), but the increased height of the shoulders relative to the central peak (see Fig. 13) indicates that the wave functions of the unpaired spins are perhaps more localized than those of the optically-induced states. In fact, the data are consistent with localization on a single As atom.

Similar behavior has recently been observed in amorphous phosphorus[94,95] where better resolution in the optically-induced spectra has allowed a more detailed interpretation. In amorphous phosphorus two metastable and characteristically different paramagnetic centers are observed by ESR after either x-irradiation or optical excitation below 77K. The ESR spectra of these

Fig. 12c and has no counterpart in the trace in Fig. 7. Of more importance is the fact that the broad features associated with the As center are much better resolved in the x-irradiated trace. This fact means that the two ESR centers are related but not identical.

In fact there are many more ESR centers created after x-irradiation than there are after low intensity optical excitation. In addition, similar features (better resolution and greater spin densities) are observed after prolonged high power ($\gtrsim$ 100 mW/cm^2) laser irradiation at band-gap energies.[90,91] Figure 13 shows the different lineshapes for As_2S_3 and Ge_2S_8 at low- and high-power optical excitation. The differences in lineshape are not well understood, but the different spin densities have been explained by Biegelsen and Street.[91] These authors examined the time dependence of the inducing process at ~ 10K before and after cycling to ~ 150K. In this manner Biegelsen and Street determined that there are two separate processes which contribute to the ESR. The first process, which dominates at low intensities and saturates near 10^{17} spins/cm^3, is due to the rearrangement of charge in existing (negative U) defects, and the second process is the creation optically of new defects The second process saturates at much higher spin densities.[90,91]

2. Pnictide Amorphous Semiconductors

In addition to the optically-induced responses discussed in the previous section, the group V amorphous solids also possess an ESR response which, even in the absence of optical excitation, increases with increasing temperature. This so-called thermally-generated ESR resonance is shown as a solid line in Fig. 14. The optically induced response (dashed line of Fig. 14) occurs only at low temperatures after optical excitation with low intensity (~ 1 mW cm^{-2}) band gap (absorption coefficient $\alpha \approx 100$ cm^{-1}) light. This resonance is exactly analogous to the broad line which is observed in the arsenic-containing

induced ESR is much better resolved and the iron scavenges essentially all of the holes[84] (trace a in Fig. 11). The increased resolution in glassy As_2O_3 allows a much more detailed model fit to the data (curves b and c) and confirms the conclusion that the unpaired electron in the As-related center is predominantly in a 4p orbital (~ 99% p character in As_2O_3).

Similar optically-induced spectra occur in IV-VI chalcogenide glasses such as GeS_2 and $GeSe_2$. In addition, similar spectra are observed after excitation with high intensity ($\gtrsim$ 100 mW/cm^2) light near the band edge or with electron- or x-irradiation. Figure 12 illustrates the ESR observed in three chalcogenide glasses after x-irradiation[33] near 77K. In GeS_2 the spectrum is actually due to two ESR centers, a hole trapped on the chalcogen and an electron trapped on a Ge atom.[86-89] These two ESR responses have analogues in the oxide glasses (GeO_2 and SiO_2). The sulfur-related center is the analog of an oxygen hole center and the Ge-related center is probably the analog of the so-called E' center of the oxide glasses. Unlike most of the chalcogenide glasses these two centers usually occur in unirradiated GeS_2 and Ge_xS_{1-x} glasses.[86] As the stoichiometry is altered the relative intensities of the Ge- and S-related ESR lines change.[86] This behavior is also seen in the Si_xO_{1-x} and Ge_xO_{1-x} systems.

As one goes from GeS_2 to $GeSe_2$ the ESR spectrum broadens considerably (compare a and b of Fig. 12). Some of this broadening is attributable to the increased spin-orbit coupling in Se, but the general lack of any resolved structure in $GeSe_2$ remains a mystery.

There are several significant differences between the x-irradiated spectra and the spectra obtained from low level ($\lesssim$ 100 mW/cm^2) optical excitation in the chalcogenide glasses. These differences are illustrated for As_2S_3 by comparison of Fig. 12c with the top trace of Fig. 7. In the x-irradiated sample there exists a sharp feature near $g \approx 2.002$ which is distorted in the trace of

The addition of most impurities to the chalcogenide glasses has little effect on the number of optically-induced ESR centers[83] but can substantially affect the type of center which is produced.[84] Figure 8 shows the relative intensity of the optically-induced ESR in As_2Se_3 as a function of Cu, Tl, K and I doping. It is apparent from this figure that these impurities have little effect on the ESR. Most other impurities exhibit similar behavior. One notable exception is oxygen in Se which dramatically reduces both the optically-induced ESR and the PL efficiency.[85] Also, it is apparent from Table 2 that the addition of As to Se increases the ESR spin density.

There is a gradual decrease in the ESR intensity with the addition of K or I (Fig. 8). In the case of iodine doping this decrease is predominantly a decrease in the intensity of the As-related center as shown in Fig. 9 (features marked A,B, C). A comparison of this trace with the middle trace in Fig. 7 indicates that the broad features associated with the As-related ESR site are diminished with respect to the narrow central feature which is associated with the Se-related center. The hole center on Se is essentially unaffected except at the highest impuritiy levels. This behavior, which occurs often in the oxide glasses, is the result of a scavenging of the electrons produced upon optical excitation by a defect which is probably assocaited with iodine. As can be seen from Fig. 8, the presence of iodine also slightly affects the charge state of the iron impurities in glassy As_2Se_3.

The opposite effect can also occur as shown in Fig. 10. When iron is added to As_2S_3 the optically induced spectrum is predominantly due to the As-related center with the chalcogen center almost completely suppressed. In this case there is an increase in the Fe^{3+} ESR after optical excitation which indicates that the Fe^{2+} has become a better hole scavenger than the S in this glass. This effect is even more dramatic in As_2O_3 where the As-related optically-

It is beyond the scope of this chapter to review all of the metastabilities which occur in amorphous semiconductors. In fact the general picture is still rather confusing for most materials. For this reason we will be content to review the most important aspects of the optically-induced ESR with reference to other optically-induced effects only when the connection is reasonably obvious.

1. Chalcogenide Glasses

When the chalcogenide glasses are irradiated at low temperatures with light of energy approximately equal to the band-gap energy, metastable ESR responses are generated. The typical inducing energies and saturated spin densities for low level excitation (~ 1-10 mW/cm^2) are listed for several amorphous semiconductors in Table 2. Typical optically-induced ESR spectra [81] observed in Se, As_2Se_3 and As_2S_3 are shown in Fig. 7. Two ESR sites contribute to the spectra in As_2Se_3 and As_2S_3 and one site in the case of Se. These ESR responses can be bleached by light of less than band gap energies ($E_g/2 \lesssim h\nu \lesssim E_g$).

The spin-Hamiltonian which describes the spectra of Fig. 7 contains the electronic Zeeman and hyperfine terms (Eqs. 1 and 3). By analyses of these spectra[81] it has been determined that the unpaired spin in Se is due to a hole localized predominantly in a p-orbital on a single Se atom. In As_2Se_3 and As_2S_3 the spectra are the superposition of two ESR responses of roughly equal spin densities. The two responses are due to the hole localized on the chalcogen atom (nonbonding or dangling bond p-orbital) and an unpaired electron localized on at most several As atoms as described in the next section.[21,81]

The optically induced ESR centers are metastable up to temperatures of ~ 50K above which they decay.[82] No contribution is observed above ~ 200K. This behavior has been attributed to a broad distribution of thermal release energies in these glasses.

evidence that doping with either P or B introduces additional localized states near the band edges, particularly near the valence-band edge.[73,79,80]

In addition to a-Si:H and doped a-Si:H, a myriad of other alloy systems based upon a-Si:H have recently been investigated. These systems include alloys of silicon (and usually hydrogen) with carbon, nitrogen, germanium, arsenic, alluminum, gold, boron or oxygen. In some studies the hydrogen has been either partially or totally replaced by flourine. With the exception of some a-Si_xC_{1-x}:H alloys most of these materials possess large ESR spin densities ($n_s \geq 10^{17}$ spins/cm^3).

D. Optically-Induced ESR

Even in amorphous semiconductors which are normally diamagnetic, such as the chalcogenide glasses, an ESR signal can usually be induced optically. At low enough temperatures this optically-induced ESR is metastable. Although the details of the ESR responses depend on the material, the common interpretation for nearly all of the observed optically-induced signals is in terms of a highly-localized "dangling bond" on one of the major constituent atoms. The most important exception to this general statement is a signal observed in the elemental pnictide amorphous semiconductors As and P which is attributed to a spin localized on two equivalent group V atoms.

There are often parallels between the behavior observed for the optically-induced ESR in amorphous semiconductors and the behavior of other experimental observations. For example, there is usually an absorption below the optical band edge which accompanies any optically-induced increase in the ESR. Sometimes there is a decrease in a characteristic, existing photoluminescence (PL) band or the appearance of a new PL band after otpical excitation. In most amorphous semiconductors many transport properties are also changed after optical excitation.

conductivity at a finite temperature) can be altered in a-Si:H alloys by doping. The doping process is similar to that which occurs in crystalline semiconductors except that the efficiency of the process is 10^{-2} to 10^{-3} instead of unity.

Additional ESR resonances are observed in doped samples of a-Si:H. Figure 6 shows the spectra whch are observed in both boron (p-type) and phosphorous (n-type) doped samples. In crystalline semiconductors at low temperatures ESR responses such as those in Fig. 6 would be attributed to electrons or holes on un-ionized donors or acceptors. In a-Si:H these signals are thought to arise from an entirely different electronic state. The most common interpretation[28] is that these resonances are due to electrons or holes trapped in the localized electronic states which occur near the band edges in amorphous solids (the so-called "band-tail" states). It has also been suggested that these resonances might arise from charged states of two-fold coordinated silicon defects.[66-68] Regardless of the explanation, the general reason for not observing ESR from un-ionized B or P impurities is that the electrons and holes are trapped by lower-lying states.

As shown in Fig. 6 the ESR line in heavily P-doped a-Si:H is narrow and centered at g = 2.004, and the line in heavily B-doped material is broader and centered at g = 2.013.[69-75] In both samples the spin densities are greater than $\sim 10^{17}$ spins/cm^3. Upon close examination Fig. 6 illustrates the fact that it is difficult to resolve the dangling bond resonance at g = 2.0055 from the resonances associated with P- and B-doping.

Studies of the temperature dependences of the resonances asscіated with P- and B-doping have provided important information concerning the conduction processes for electrons and holes trapped in localized states near the band edges.[76] Other studies of these resonance have provided the basis for a determination of the densities of band-tail states[77,78] in a-Si:H. There is

is temperature dependent. The first contribution is usually attributed to exchange effects between spins[52] and the second to site-to-site hopping of the spins themselves.[51,53-56] The hopping term can be correlated in some cases with electrical conductivity measurements.[47,51,57,58]

As substantial amounts of impurities are added to a-Si or as a-Si is alloyed with other elements, changes sometimes occur in the ESR responses. The incorporation of oxygen reduces the spin density to levels in the order of $n_s \sim 10^{18}$ spins/cm^3.[59] Manganese impurities also reduce n_s to levels on the order of $\sim 10^{17}$ spins/cm^3 presumably because the Mn^{2+} paramagnetic ions have donated electrons to the Si dangling bonds.[60] By far the most dramatic effect occurs on the incorporation of substantial (1-30 at. %) amounts of hydrogen where n_s can be as low as $\sim 10^{15}$ spins/cm^3 under optimal conditions. Such materials are really silicon-hydrogen alloys and usually denoted as a-Si:H.

In a-Si:H the ESR lineshape ($\sigma \sim 7.5$ G) and g-value ($g = 2.0055$) are essentially the same as those observed in a-Si for $n_s \lesssim 10^{19}$ spins/cm^3. In fact, by varying the hydrogen content either through varying the deposition conditions[61,62] or through annealing at elevated temperatures[61,63] one can vary the ESR spin density by several orders of magnitude and yet the lineshape and g-value remain remarkably unchanged. One might a priori expect that the introduction of $\sim$ 10 at. % hydrogen would tend to broaden the observed ESR line through the hyperfine interaction between H and the unpaired spins (Eq. (3)). The fact that this broadening does not occur implies that the unpaired spins are indeed highly localized on Si atoms.[64] Similar results are observed in the a-Si:F system.[65]

In the a-Si:H alloy system the drastic reduction of the ESR signal implies that most of these states near the middle of the energy gap are removed. This drastic reduction in deep gap states means that the Fermi level (and hence the

silicon "dangling bond." This identification rests in part on an analogy with a similar signal seen on clean 111 surfaces of crystalline Si,[46] with similar sites in the bulk of single crystal silicon,[47] and with similar sites on Si-SiO_2 interfaces.[48] While there reamin some minor unexplained complications,[49] there is strong evidence for the identification of the ESR response which occurs in a-Si and also in a-Si with hydrogen, as an electron trapped in a dangling bond orbital of a three-fold-coordinated silicon atom.

Amorphous Si is known to be an inhomogeneous and anisotropic material with internal voids whose sizes and shapes vary depending on the method of preparation. It has often been suggested that the spins in a-Si reside on the internal surfaces of these voids although this is not a universally accepted interpretation.[23,50] Because the spin density depends in a complicated fashion on the exact conditions for preparation, it is difficult to find a general description for the microscopic morphology in the region of the dangling bonds. Most likely there are several ways of incorporating this defect.

At lower spin densities ($< 10^{19}$ spins/cm^3) the ESR lineshape is essentially temperature independent but does depend on the spin density. Three possible contributions to this linewidth are anisotropies in the g-tensor, variations in the g-values at different paramagnetic sites and the dipolar interaction between spins (see Eq. (6) below). It has proved difficult to separate these three contributions unambiguously, but the bulk of the evidence suggests that at least at the lowest spin densities ($n_s \sim 10^{18}$ spins/cm^3) the first two mechanisms dominate.[23,51] Any broadening due to the g-tensor should scale linearly with the frequency at which the measurement is made, and this dependence has been observed in some cases.[23,51]

At spin densities greater than 10^{19} spins/cm^3 in a-Si there is a narrowing of the temperature-independent ESR linewidth and an additional component which

decays rapidly above ~ 90 K, is presumably due to the trapping of a hole at NO_2^- radicals after x-irradiation. The NO_2^- radicals thus serve as (presumably shallow) hole traps in a-Si:H.

Shimizu et al.[41] have investigated the influence of transition metal ions on the ESR in a-Si:H films. In these studies ESR responses from Fe, Mn and Ni were observed. Only a small fraction of the total transition metal impurities is observed to contribute to the ESR. The explantion of this result is unclear.

C. ESR in Tetrahedral Amorphous Semiconductors

The tetrahedral amorphous semiconductors which have been studied in the most detail are those based upon amorphous silicon (a-Si) or its alloys (a-Si:H, a-Si_xGe_{1-x}:H, a-Si_xC_{1-x}:H and so forth). In addtion, there have been some investigations of amorphous germanium (a-Ge) and glassy $CdGeAs_2$.

In the case of a-Si there is always a strong ESR response which corresponds to $\geq 10^{19}$ spins/cm^3 regardless of the method of preparation. This ESR response which was first observed by Brodsky and Title,[42] is a narrow essentially symmetric line centered near g = 2.0055. At the lowest spin densities ($< 10^{18}$ spins/cm^3) the lineshape becomes asymmetric.[43]

Because a-Si can only be made in thin-film form, early experiments were designed to establish that the ESR signal was predominantly a bulk effect.[42,44] Early experiments on samples evaporated under ultra-high-vacuum conditions also established that the characteristic ESR signal was not due to impurities.[45] These two facts imply that the ESR signal is due to an "intrinsic" property of a-Si.

Although there is little detail in the ESR spectrum with which to make an unambiguous identification of the microscopic origin of the signal, a qualitative picture has emerged. This picture, which is essentially that suggested by Brodsky and Title in their original paper,[42] is that the signal arises from a

dangling bonds. This increase depends on the initial ESR spin density and is less important in those films with the lowest initial spin densities, Street and Knights[38] interpret these increases as due to the diffusion of oxygen into internal surfaces with the consequent changes in local bonding arrangements producing an increase in the number of Si dangling bonds on these internal surfaces.

In more recent studies, Pontuschka et al.[39] have reported ESR from several impurity species in a-Si:H films. In films intentionally doped with ~ 2 at. % O and ~ 0.1 at. % N these authors observe the ESR responses shown in Fig. 5 after x-irradiation at 77 K. The sharp doublet lines separated by ~ 500 G are due to atomic hydrogen which is trapped in oxygen-rich cages. This resonance is not observed in undoped films. The signal decays above ~300 K as the atomic hydrogen begins to move and combines with other atomic hydrogen to form molecular hydrogen. The molecular hydrogen presumably diffuses out of the films.

In addition to atomic hydrogen there are ESR responses near g = 2.0 in Fig. 5 due to silicon-oxygen hole centers (holes trapped on singly-coordinated oxygen atoms, broad line), silicon dangling bonds and silicon E' centers (electrons trapped on sp^3-hybridized silicon orbitals at sites where the silcon atoms are bonded to three oxygen atoms, narrow line).

Tight-binding calculations[40] suggest that isolated Si-O configurations in a-Si:H do not give states in the gap. These results imply that the oxygen is clustered in these films to produce SiO_x-rich regions, and the most likely places for these SiO_x-rich regions are on the internal surfaces of voids.

In some "undoped" films which were x-irradiated at 77 K, Pontuschka et al.[39] also observed an ESR spectrum which they attributed to trapped NO_2 molecules, but these authors were unable to reproduce this spectrum in a fashion which could be correlated with sample preparation conditions. This ESR signal, which

Features are again observed at g ≈ 4.2 and g ≈ 2.0 with the feature at 4.2 showing a resolved hyperfine structure and the one at 2.0 being motionally narrowed with no resolved structure. The 4.2 feature is probably characteristic of Mn^{2+} in the chalcogenide glasses but the feature at 2.0 has been attributed to polycrystalline MnO precipitates in the glassy matrix.[36]

The ESR studies of transition metal impurities in the chalcogenide glasses have not yielded the rich structural information often obtained from other ESR studies. There are several reasons for this lack of success. First, the strong fine structure interaction (Eq. 4) in these paramagnetic species broadens the ESR lineshapes such that comparisons with models are difficult to make.[34] Second, substantial statistical distributions of the spin-Hamiltonian parameters occur such that it is difficult to find unique parameters to fit a given ESR spectrum. In addition, the ESR spectra are often essentially independent of the host glass which means that little structural information specific to a given glass can be obtained. As a result of these difficulties studies of transition metal impurities in chalcogenide glasses have not been as successful as ESR probes of other paramagnetic species in these glasses.

2. Tetrahedral Amorphous Semiconductors

In a-Si the earliest detailed ESR experiments on the influence of impurity species were performed by Miller and Haneman.[37] These authors studied O_2 diffusion into a-Si films and discovered that the O_2 greatly increases the spin-lattice relaxation rates (see Section III.D) for the characteristic ESR response with g = 2.0055. These results are interpreted as suggesting that the spins contributing to this ESR response are located primarily on the internal surfaces of voids which are accessible to oxygen diffusion.

In hydrogenated amorphous silicon, on the other hand, Street and Knights[38] find that exposure to air increases the ESR spin density associated with silicon

mentioned previously, most of the iron in nominally pure As_2S_3 or As_2Se_3 is in the 2+ valence state. As one adds most metallic impurities to these glasses, some Fe^{2+} is converted to Fe^{3+} when the metallic doping levels exceed the intrinsic concentration of iron impurities. This situation is shown for As_2Se_3 in Fig. 4. At high doping levels (~ 0.1 - 1.0 at.%) the Fe^{3+} ESR response is increased by over an order of magnitude from that observed in the undoped glass. This trend is the opposite of that observed[1] by susceptibility measurements in As_2S_3, a discrepancy which is not understood.

Copper, which is also a pervasive and inadvertent impurity in may chalcogenide glasses, can also exist in paramagnetic form. In the case of Cu in As_2Se_3 where the bonding is known form XAFS to be tetrahedral,[32] the predominant valence state is probably diamagnetic Cu^{1+} independent of the copper concentration. A small fraction of the copper (10^{16}-10^{17} cm^{-3}) can exist as Cu^{2+} in octahedral coordination when materials are made under nonequilibrium conditions (films evaporated onto 300K substrates or boules rapidly quenched from the melt) as indicated in Fig. 3. X-irradiation also produces similar concentrations of Cu^{2+} when substantial copper is present ($\gtrsim$ 0.1 at.% Cu).[30] The octahedral Cu^{2+} in As_2Se_3 definitely does not represent the equilibrium situation because the ESR signal is greatly reduced after annealing at 180°C for one hour. There may also be some evidence for the existence of tetrahedral Cu^{2+} in As_2Se_3 films evaporated onto 300K substrates.[30] Unlike Fe^{3+}, the magnitude of the Cu^{2+} signal does not appear to depend on doping with other impurities but only on the nature of the non-equilibrium preparation conditions.[30,33]

A third transition metal impurity which has been studied extensively in the chalcogenide glasses is manganese.[34] Like the Cu^{2+} and Fe^{3+} cases, the Mn^{2+} spectrum is essentially independent of the host chalcogenide glass.[35,36]

the chalcogenides and pnictides, however, most of the optically-induced signals are transient and disappear after the removal of the exciting light. In undoped samples the transient optically-induced ESR signals arise from localized electronic sites near the conduction (g = 2.004) and valence (g = 2.013) band edges.[99,100] The top trace in Fig. 16 shows a typical spectrum for undoped a-Si:H.

The middle trace in Fig. 16 shows the spectrum observed during optical excitation in heavily p-type (B-doped) samples. In these films the hole valence-band-tail resonance (g = 2.013) and the resonance attributed in section III.C to silicon dangling bands (g = 2.0055) are observed. In heavily n-type (P-doped) a-Si:H only the dangling bond resonance is observed on optical excitation (bottom trace in Fig. 16). It is clear from Fig. 16 that the overlap between these various resonances as well as their featureless nature makes it difficult to make an unambiguous identification of the specific ESR responses; nonetheless, the interpretation presented is the most commonly accepted.[100] In all studies the silicon dangling-bond resonance is observed to increase with either P- or B-doping. The resonance due to holes trapped in the valence band tails occurs only in undoped or B-doped films while that due to the electrons trapped in conduction band tails is only observable in undoped films. There is a broad distribution of decay times for these resonances ranging from 0.1 to greater than 10^3 sec.[101] The intensities in Fig. 16 are, of course, not an absolute indication of the spin densities because the observed amplitudes are dynamical balances between excitation and decay processes.

The dependence of the transient light-induced ESR intensity on the intensity of the exciting lgiht is less than linear over many orders of magnitude.[102,103] The explanation for this dependence is still controversial. It was originally suggested that the effect resulted from optical saturation of the longer-

lived geminate pairs of trapped electrons and holes,[102] but recently it has also been suggested that distant pairs of trapped electrons and holes may be responsible.[103]

Two model explanations for the transient light-induced effects have been suggested. The most commonly accepted model is that the electron and hole resonances at g = 2.004 and g = 2.013 are due to electrons or holes trapped at strained bands in the conduction or valence-band tails, respectively.[100,104] The observation of the various ESR lines then depends on the position of the Fermi level with respect to these bands. The second model suggests that these two resonances are due to negatively or positively charged states of two-coordinated silicon atoms which form a positive U system where the ground states are charged.[66]

In addition to the transient, optically-induced ESR in a-Si:H there is also a metastable component, a part of which exists for long times only below ~ 80K[73] and a part of which is stable at temperatures up to ~ 400K.[74,76,105] Similar effects have also been observed following x-irradiation.[39] Recently several experiments have probed the kinetics of this metastable optically-induced ESR,[106-108] but the results are still somewhat controversial. One point is clear, however. At high enough intensity of the exciting light large numbers (~ 10^{18}-10^{19} spins/cm^3) of paramagnetic states can be created, which are presumably due to the optically-induced creation of dangling bonds[74,76,107] just as occurs at high powers in the chalcogenide glasses (at lower temperatures).

E. Spin-Lattice Relaxation

Spin-lattice relaxation in electron spin resonance is the process by which the ensemble of paramagnetic spins transfers energy to the lattice after microwave excitation in a magnetic field. The relaxation process is often

exponential and hence can be characterized by a rate T_1^{-1} where T_1 is the spin-lattice or longitudinal relaxation time. Measurements of T_1 as functions of temperature, magnetic field, and spin density often provide important insights into the mechanisms that govern the coupling of paramagnetic spins to the amorphous network.

Little detailed information has been published concerning spin-lattice relaxation rates of the ESR in the chalcogenide and pnictide amorphous semiconductors. In As_2Se_3 both the Se- and As-related centers relax on times on the order of $T_1 \sim 0.1$ msec at $\sim$ 4K.[21] In amorphous As the times at this temperature are approximately a factor of three faster, while in amorphous phosphorus they are at least a factor of five slower.[21,95] With the possible exception of amorphous P, these values of T_1 are at least an order of magnitude faster than values commonly encountered in crystalline materials at the same spin densities. The origin of the increased relaxation rates is probably the presence of anomalous low-frequency tunneling or "disorder" modes in the glasses. The effect of such modes on the NMR spin-lattice relaxation rates will be discussed in section IV.B.

In the tetrahedral amorphous semiconductors, more extensive measurements of T_1 have been peformed, particularly on films of a-Si and a-Si:H. In a-Si the spin densities are always > 10^{18} spins/cm^3 and the relaxation is often controlled at high temperatures ($\gtrsim$ 150K) by the hopping of electrons.[56,109,110] At lower temperatures (T < 100K) T_1 is proportional to the temperature and the relaxation is dominated by phonons (so-called direct processes).[56,109] In some films of a-Si and in most films of a-Si:H the dominant relaxation process at high temperatures (T > 100K) is thought to be due to tunneling or disorder modes.[111]

IV. NMR AND NQR

In the chalcogenide and pnictide amorphous semiconductors nuclear magnetic resonance (NMR) and nuclear quadruple resonance (NQR) have been used effectively to probe the local bonding arrangements of major constituent atoms. In addition, studies of the changes in local structural order after the application of light in chalcogenide films have provided useful information concerning photostructural processes in these films. Measurements of nuclear spin-lattice relaxation have provided evidence for the existence of highly anharmonic tunneling modes in the chalcogenide and pnictide amorphous semiconductors.

The NMR measurements on the tetrahedral amorphous semiconductors have also yielded useful information converning local structural order primarily for the hydrogen atoms in a-Si:H. For example, these measurements have provided detailed local information concerning the inhomogeneities present in a-Si:H films. In addition, some defects such as trapped H_2 molecules have been inferred from NMR measurements in a-Si:H.

The important terms in the Hamiltonian which decribes most NMR and NQR applications are the nuclear Zeeman, the dipolar, the chemical shift or Knight shift, and the quadrupolar interactions. The nuclear Zeeman interaction can be written in the form

$$H_{nz} = -\gamma\hbar\vec{I}\cdot\vec{H} \tag{5}$$

where γ is the nuclear gyromagnetic ratio.

The dipolar interaction between nuclear spins is of the form

$$H_d = \frac{1}{2} \sum_j \sum_k \left[\frac{\vec{\mu}_j\cdot\vec{\mu}_k}{r_{jk}^3} - \frac{3(\vec{\mu}_j\cdot\vec{r}_{jk})(\vec{\mu}_k\cdot\vec{r}_{jk})}{r_{jk}^5} \right] \tag{6}$$

where the primes denote $j \neq k$, $\vec{r}_{jk}$ is the radius vector from $\vec{\mu}_j$ to $\vec{\mu}_k$, and the magentic moments $\vec{\mu}_j$, $\vec{\mu}_k$ are given by $\vec{\mu}_{j,k} = \gamma_{j,k}\hbar\vec{I}_{j,k}$.

The dipolar Hamiltonian of Eq. (6) is usually too complicated to evaluate exactly, so one must often resort to approximate methods of evaluation. One approach often used is to abandon any attempt to calcualte the lineshape and merely calculate the second moment M_2 which is given by

$$M_2 = \frac{3}{5}\gamma\hbar^2 I(I+1) \sum \frac{1}{r_{ij}} \tag{7}$$

wehre r_{ij} is the distance between nuclei i and J. For concentrated spins ($\gtrsim$ 5-10 at.%) the dipolar lineshape is expected to be Gaussian and the full width at half maximum is given by

$$\sigma_{FWHM} = [8(\ell n\ 2)M_2]^{1/2} . \tag{8}$$

For dilute systems a Lorentzian lineshape is expected and

$$\sigma_{FWHM} = \frac{4\pi^2}{3\sqrt{3}}\gamma^2\hbar n \tag{9}$$

where n is the density of nuclear spins.

The chemical shift interaction results when the electronic Zeeman contribution polarizes the electronic spins, which in turn interact via their orbital and spin components with the nuclear spins. Both diamagnetic and paramagnetic contributions to the local magnetic field as seen by the nucleus, can be generated in this fashion. This interaction is, in general, very complicated because it involves many of the electrons in the solid. In practice one usually writes the chemical shift Hamiltonian in parameterized form as

$$H_C = \gamma\hbar\vec{I}\cdot\bar{\sigma}\cdot\vec{H} \tag{10}$$

where $\bar{\bar{\sigma}}$ is the chemical shift tensor which depends on the local order in the solid. Structural information can be obtained from $\bar{\bar{\sigma}}$ either by comparison with situations of known bonding or by analyzing trends.

A quadrupolar contribution to the Hamiltonian can exist whenever the nucleus has spin I greater than 1/2 (non-spherical nucleus). For nuclei with $I > 1/2$ this term is often the second most important one next to the nuclear Zeeman term. In some cases the quadrupolar term dominates over all terms and no externally-applied magnetic field is required to perform the resonance experiments. This situation is called nuclear quadrupole resonance or NQR.

When the nucleus is not spherical, the electric quadrupole moment of the nucleus is coupled to the gradient of the electric field at the nuclear site. This electric field gradient is due predominantly to the bonding electrons. The quadrupolar Hamiltonian is ususally written in parameterized form as

$$H_Q = \vec{I} \cdot \bar{\bar{Q}}' \cdot \vec{I} \qquad (11)$$

where the quadrupolar tensor $\bar{\bar{Q}}'$ can be expressed in terms of only two independent parameters eq and η. The parameter eq is the largest diagonal component of the electric field gradient tensor at the nuclear site. The parameter η is a measure of the asymmetry of this tensor (departure from axial symmetry) and runs from 0 to 1.

Just as in the case of ESR described in Section III, the NMR of polycrystalline or amorphous samples consists of sums over sites whose principal axes are randomly oriented with respect to the applied field. In amorphous solids these powder patterns may also be modified by distortions which vary from site to site.

A. Local Bonding Probes

Historically, perhaps the most important contribution of NMR or NQR to solids has been in determining details of the local structural order. For this purpose the chemical shift interaction can be used to understand trends in bonding. Of greater utility, when it exists, is the quadrupolar interaction from which one can often develop detailed models of the wave functions of the bonding electrons. Sometimes the dipolar interaction is useful in distinguishing between different local environments for nuclei in solids.

1. Chalcogenide Glasses

For technical reasons NMR in the chalcogenide glasses is particularly difficult to observe. In the case of selenium this difficulty results from the particularly low isotopic abundance of ^{77}Se, the major isotope with a non-zero nuclear spin.

The ^{77}Se NMR spectra[113] observed in various forms of Se are shown in Fig. 17. All traces represent the derivative of the absorption spectrum. The vertical line on the left represents the position of the ^{77}Se NMR in a 10 molar solution of H_2SeO_3 in water which serves as an arbitrary standard. Chemical shifts of the ^{77}Se NMR in the various forms of Se can be measured with respect to this standard. The relative intensities of the spectra in Fig. 17 have been adjusted arbitrarily but their positions on the field scale are as shown.

A representative single crystal Se spectrum is also shown in Fig. 17 with the c-axis perpendicular to the direction of the applied magnetic field, and a strong angular dependence of the resonance position was observed as the crystal was rotated about the c-axis. This angular dependence is characteristic of an anisotropic chemical shift tensor which is expected for the case of strongly directed covalent bonds (Eq. (10)). In the powdered crystalline trace the intensity is averaged over all orientations of the chemical shift tensor

relative to the magnetic field as in the case of a glass, and this is the appropriate spectrum for comparison with that of glassy Se.

The spectrum observed in solid glassy Se shown at the top of Fig. 17 has a width of 3.3 G and an isotropic component of the diamagnetic chemical shift of 0.064 percent relative to the 10 kG H_2SeO_3 standard. The position of the zero-crossing of the derivative curve is used to define the isotropic chemical shift. Because of the low isotropic abundance of ^{77}Se, the dipolar contributions to the line width are negligible.

The structure of glassy Se is usually assumed to be a mixture of the helical chains of trigonal Se and the 8-membered ring molecules of α-monoclinic Se. However, since the bonding configuration in the rings and chains differs only in the second nearest neighbor, the NMR spectra of these two modifications should be quite similar. On this basis one might have expected greater similarity in the NMR spectra of powdered trigonal Se and glassy Se since in both cases all orientations of the chemical shift tensor relative to the magnetic field are present. However, the statistical variations in bond length and angle characteristic of vitreous materials accounts for the observed differences.

In solid glassy As_2Se_3, a symmetric ^{77}Se NMR spectrum is observed with a width of 6.2 G and diamagnetic isotropic chemical shift of 0.111 percent with respect to the H_2SeO_3 spectrum.[114] The substantial difference between the isotropic chemical shifts of the ^{77}Se NMR in glassy Se and As_2Se_3 makes it possible, in principle, to distinguish between Se-Se and As-Se bonds in mixed chalcogenide glass systems containing Se and As.

In molten Se the width of the ^{77}Se NMR spectrum (see Fig. 17) is reduced to the limit of the magnetic field inhomogeneity ($\sim$ 0.1 G), and the measured isotropic diamagnetic chemical shift of 0.042%, roughly 40% less than that of solid glassy Se. The observation of this narrowed resonance in molten Se means

that the spectral broadening caused by the site-to-site variation in the chemical shift interaction in solid glassy Se has been averaged essentially to zero by the atomic motion or reorientation in the melt. This phenomenon, called motional narrowing, occurs when the correlation time for the bonds involving the resonant nuclei, becomes as short as the reciprocal of the rigid lattice linewidth expressed as a frequency. The occurrence of the motional narrowing implies that the covalent intrachain bonds of the liquid Se are being disrupted at 220°C in liquid Se.

The motional narrowing of the ^{77}Se NMR in liquid Se is in striking contrast to the Tl^{205} NMR results in thallium-containing layer-structure glasses where no changes are observed[115] in either the chemical shift or the linewidth for temperatures in the molten phase well above T_g. Futhermore, no motionally narrowed ^{77}Se NMR is observed in molten layer-structure As_2Se_3 at temperatures ranging up to 400°C where its viscosity is equivalent to that of Se at 220°C. In these layer-structure materials motional narrowing does not occur. Hence the the temperature dependence of the NMR spectra in solid and liquid chalcogenide glasses provides evidence that faster atomic reorientation rates occurs in molten chain-structure glasses than in molten layer-structure glasses at equivalent viscosity.

In addition to ^{77}Se NMR, several other nuclei in the chalcogenide glasses have been investigated. The thallium NMR (^{203}Tl and ^{205}Tl) in Tl-As-Se glasses serves as an illustrative example.[115] When the chemical shift of Tl is investigated in the system $(Tl_2Se)_x(As_2Se_3)_{1-x}$, there is a sharp change in this shift near $x = 0.3$ as shown in Fig. 18. One will note from this figure that relatively large paramagnetic, isotropic chemical shifts are observed for high thallium content ($x > 0.3$) which indicate that the thallium bonding configuration in these glasses is very covalent. At lower thallium content there is

a sharp transition to a less covalent bonding configuration. Although the evidence is not conclusive, it has been suggested[115] that these chemical shift results indicate that the thallium atoms enter the glass as Tl^{1+} ions for low thallium content but assure the Tl^{3+} valence state at high Tl content ($x > 0.3$).

In the arsenic chalcogenide glasses the ^{75}As NMR can be studied by NQR techniques. In As_2S_3 and As_2Se_3 glass the NQR line is very broad (~ 4-10 MHz) in comparison to the lines in the crystalline forms ($\lesssim$ 50 kHz).[116] The spectrum[117] for glassy As_2Se_3 is shown in Fig. 19. It has been pointed out[115] that although the line is very broad, the quadrupolar interaction (Eq. (11)) is so sensitive to small changes in local bonding configurations that the As sites are still very well defined in these glasses. Crude estimates of the distortions from the average of the pyramidal apex bonding angles for the As sites range from ~ 1° to ~ 5° in As_2S_3 and As_2Se_3 glasses. It is clear from Fig. 19 that the As pyramids in glassy As_2Se_3 are very similar to those which exist in layered, crystalline As_2Se_3 and very different from the As sites in crystalline As_4Se_4 which has a molecular structure.

One can thus infer real similarities in the local As bonding between glassy and crystalline As_2S_3 and As_2Se_3 from the observed NQR. In particular[116,117] the ring structure in crystalline As_2S_3 (As_2Se_3) is by and large preserved in the glassy phase.

From the ^{75}As NQR measurements one cannot determine both the quadrupolar coupling constant e^2qQ/h (where Q is the quadrupole moment of the As nucleus) and the asymmetry parameter η independently. However, experiments in the presence of a magnetic field (Zeeman perturbation where $H_Q >> H_{nz}$ in eqs. (5) and (11)) do provide an independent measure of η.[118,119] These measurements indicate that there are at least two predominant values for η in glassy As_2S_3 and As_2Se_3 ranging from $\eta \approx 0$ to $\eta \approx 0.4$. The exact shape of the distribution

of values of n in As_2S_3 and As_2Se_3 is still a controversial point.

The parallels between crystalline and glassy forms of A_2B_3 chalcogenides also extend to As_2O_3 as shown in Fig. 20. The ^{75}As NQR spectrum in glassy As_2O_3 is centered about the position of the NQR in the layered, claudetite form of As_2O_3 and not about the molecular, arsenolite cyrstalline modification. Once again the existence of the ring structure on glassy As_2O_3 can be inferred from the NQR results.

One additional use of ^{75}As NQR to determine local structural order in chalcogenide glasses must be mentioned. In fast evaporated films of As_2S_3 and As_2Se_3 the NQR spectra are very different from those observed in the bulk glasses. In these films there is substantial NQR intensity in the regions where As_4S_4 and As_4Se_4 lines occur in the crystalline forms (see Fig. 19). Upon application of light at band gap energies these As_4S_4 or As_4Se_4 sites in the glassy films can be irreversibly photopolymerized into sites resembling those in the bulk, annealed glass.[120] One can then use ^{75}As NQR to monitor these photostructural changes in the chalcogenide glasses. In well-annealed, bulk glasses there is no dramatic photostructural effect[117] as indicated for As_2Se_3 by the data before and after optical excitation in Fig. 19.

2. Pnictide Amorphous Semiconductors

An ^{75}As NQR lineshape has also been observed[121,122] in amorphous As. (See Fig. 21a.) This figure also indicates schematically the lineshape observed in orthorhombic arsenic (or-As) at 4.2K. In the common form of semimetallic arsenic, which is rhombohedral (rh-arsenic), the NQR frequency falls well outside the range of Fig. 21a. The lineshape of a-As was also evaluated at 77K, and there was no discernible difference in shape at the two different temperatures. The a-As lineshape differs from those observed for ^{75}As in glassy As_2Se_3 and As_2S_3 in two respects. First, the a-As lineshape is asymmetric

(skewed to lower frequencies) while the lineshapes in As_2S_3 and As_2Se_3 are symmetric within experimental error.[117] Second, the NQR absorption in a-As occurs at frequencies which are well removed from those of either crystalline modification while the lineshapes in glassy As_2S_3 and As_2Se_3 are centered about the median of the NQR responses observed in the corresponding, crystalline, layered compounds.

The broad asymmetric lineshapes shown in Fig. 21a for a-As can be explained in terms of orientational distributions of bonding electrons on nearest neighbor atoms. Because a-As is an elemental material and all sites are chemically equivalent, there is to first order no charge transfer from one atom to another. Therefore the total charge on any atom must be essentially zero. However, there will be a charge distribution on nearest neighbor atoms which will create an additional electric field gradient (EFG) at the site of the central atom. A calculation has been performed[121] to estimate the magnitude of this effect and the resuls are shown in Fig. 21b. The contribution to the EFG from nearest-neighbor atoms in a-As was obtained by varying the dihedral angle between nearest-neighbor arsenic atoms according to the distribution functions suggested in various continuous random network models.[123] The dihedral angle distribution used in Fig. 21b is shown in the inset. The degree of asymmetry of the calculated NQR lineshape depends upon the asymmetry of the dihedral angle distribution.

It can be seen that this very simple model for the effects of outside atoms on the EFG explains the observed asymmetry of the NQR lineshape. The magnitude of the observed linewidth, however, it not well reproduced, and more sophisticated model calculations are needed.

The phosphorus nucleus does not have a quadrupole moment so one cannot obtain the same detailed information concerning bonding as was deduced for

amorphous As. Nonetheless, measurements of the chemical shift analogous to those described above for thallium indicate that the short range order of amorphous P is similar to that which exists in black phosphorus[124] and very different from the local atomic arrangement in white P.

3. Tetrahedral Amorphous Semiconductors

Most of the NMR measurements in the tetrahedral amorphous solids involve investigations of hydrogen in a-Si:H and related alloys. In the first reported measurements, Reimer et al.[125] concluded from the dipolar lineshapes and linewidths that the hydrogen atoms in a-Si:H are spatially distributed in an inhomogeneous fashion. This basic conclusion, that there are at least two different spatially separated environments for the bonded hydrogen in a-Si:H, has since been confirmed by others.[126,127] The evidence comes primarily from the ^{1}H NMR free induction decay lineshapes, a typical example of which is shown in Fig. 22. The decay of the magnetization in time contains two components which by Fourier transformation become two separate lineshapes in frequency space (inset to Fig. 22).

In Fig. 22 the initial rapid decay transforms into a broad Gaussian lineshape in frequency and the exponential time decay into a narrower Lorentzian lineshape. The widths of these two lines are governed by the dipolar term in the Hamiltonian (Eq. (6)). Several experiments have confirmed that the hydrogen atoms comprising these two lines are in general spatially separated from one another.[112,125] Essentially all films of a-Si:H exhibit these two distinct ^{1}H NMR lines. The two lines have even been observed in microcrystalline films.[128] This latter fact demonstrates that the microstructure which gives rise to the two sites can exist in both crystalline and amorphous films.

The cause of these separate and ubiquitous ^{1}H NMR lines is not extremely clear, but there are several facts upon which there is general agreement. First,

most estimates place the average separation of the two types of sites at > 5 Å although the exact value is difficult to determine.[129] Second, it is generally accepted that the narrow Lorentzian line is due to dilute hydrogen atoms either randomly situated[127,129] or slightly clustered[112] at monohydride bonding sites (tetrahedrally coordinated Si atoms which are bonded to only a single H atom and sometimes denoted as SiH sites). The narrow line constitutes about 3 at.% of the film in most cases and is rarely greater than 10 at.%.[125,127]

A third important fact concerning these two lines is that their relative proportions may vary, the intensity of the broad line generally increasing with hydrogen content. The linewidths of the lines corresponding to each site are constant within factors of approximately two. These facts suggest that the degree of clustering is essentially independent of the hydrogen content and the preparation conditions.

The interpretation of the broad line is more ambiguous. This line occurs in films in which infrared absorption measurements confirm that dihydride (SiH_2) and trihydride (SiH_3) bonding sites exist as well as in films in which only monohydride (SiH) sites are present. Evidently many kinds of clustered environments can contribute to the broad line. A common interpretation of this line, based on second moment calculations (see Eq. (7)), is that it is due to hydrogen atoms bonded on the internal surfaces of small voids.[112,129,130]

Deuterium has been substituted for hydrogen in one or two films, and the quadrupole moment of the deuterium provides an additional probe of the local bonding arrangements.[131] A quadrupolar broadened line (Pake doublet) is observed whose width agrees with the observed vibrational frequency of deuterum in a-Si:H,D. A narrow line is also observed whose origin is not completely determined but is partially due to D_2 molecules trapped in the film.[132]

49. Taylor, P.C., Magnetic resonance measurements in a-Si:H, in Semiconductors and Semimetals, Vol. 21C, Hydrogenated Amorphous Silicon, Pankove, J.I., ed., Academic Press, NY, 1984, 99.

50. Thomas, P.A. and Kaplan, D., Clustered versus distributed spins in amorphous silicon, in AIP Conf. Proc., 31, 85, 1976.

51. Voget-Grote, U., Stuke, J., and Wagner, H, Electron spin resonance of amorphous silicon, in AIP Conf. Proc., 31, 91, 1976.

52. Bachus, R., Movaghar, B., Schweitzer, L., and Voget-Grote, U., The influence of the exchange interaction on the ESR linewidth in amorphous silicon, Philos. Mag., B39, 27, 1979.

53. Brodsky, M.H., Title, R.S., Weiser, K., and Pettit, G.D., Structural, optical, and electrical properties of amorphous silicon films, Phys. Rev., B1, 2632, 1970.

54. Bahl, S.K. and Bhagat, S.M., Properties of amorphous silicon films--dependence on deposition conditions, J. Non-Cryst. Solids, 17, 409, 1975.

55. Movaghar, B., and Schweitzer, L., ESR and conductivity in amorphous germanium and silicon, Phys. Status Solidi B80, 491, 1977.

56. Thomas, P., and Flachet, J.C., Conductivity measurements on UHV deposited amorphous silicon, J. Phys. Colloq., Orsay, Fr., 42-C4, 151, 1981.

57. Voget-Grote, U., and Stuke, J., ESR spectrum of amorphous silicon, J. Electron. Mater., 8, 749, 1979.

58. Hasegawa, S., and Yazaki, S., Connection between ESR and electrical conduction in amorphous Si films, Solid State Commun., 23, 41, 1977.

59. Kubler, L., Jaegle, A., and Koulmann, J.J., The effect of oxygen on the properties of evaporated amorphous silicon: ESR studies, Phys. Status Solidi, B95, 307, 1979.

of SiO_2 and Its Interfaces, Pantelides, S.T., ed., Pergamon, N.Y., 1978, 321.

41. Shimizu, T., Kumeda, M., Watanabe, I., and Noumi, Y., ESR of transition metals in a-Si, J. Non-Cryst. Solids, 35 + 36, 645, 1980.

42. Brodsky, M.H., and Title, R.S., Electron spin resonance in amorphous silicon, germanium and silicon carbide, Phys. Rev. Lett. 23, 581, 1969.

43. Title, R.S., Brodsky, M.H., and Cuomo, J.J., Electron paramagnetic resonance study of amorphous silicon with low spin concentration, in Amorphous and Liquid Semiconductors, Spear, W.E., ed., University of Edinburgh, Edinburgh, Scotland, 1977, 424.

44. Suzuki, M., Maekawa, T., Nakao, A., Kumeda, M., and Shimizu, T., Adsorption effects on ESR and conductance of rf sputtered a-Si films, Solid State Commun. 36, 393, 1980.

45. Thomas, P.A., Lepine, D., and Kaplan, D., In situ observation of electron spin resonance in evaporated amorphous silicon, in AIP Conf. Proc., 20, 47, 1974.

46. Haneman, D., Electron paramagnetic resonance from clean single-crystal cleavage surfaces of silicon, Phys. Rev., 170, 705, 1968.

47. Title, R.S., Brodsky, M.H., and Crowder, B.L., Electron paramagnetic resonance studies in amorphous silicon, in Proc. Int. Conf. Phys. Semicond., Keller, S.P., ed., Nat. Tech. Inf. Serv., Springfield, VA, 1970, 794.

48. Caplan, P.J., Poindexter, E.H., Deal, B.E., and Razouk, R.R., ESR centers, interface states, and oxide fixed charge in thermally oxidized silicon wafers, J. Appl. Phys., 50, 5847, 1979.

31. Bishop, S.G., and Taylor, P.C., Iron impurities as non-radiative recombination centres in chalcogenide glasses, Philos. Mag., B40, 483, 1979.

32. Hunter, S.A., Bienenstock, A., and Hayes, T.M., EXAFS studies in glassy Cu-As-Se alloys, in The Structure of Noncrystalline Materials, Gaskell, P.H., ed., Taylor and Francis, London, 1977, 73.

33. Taylor, P.C., Strom, U. and Bishop, S.G., Paramagnetism in x-irradiated chalcogenide glasses and crystals, Solar Energy Mat., 8, 23, 1982.

34. Taylor, P.C., Resonance effects in glass, in Treatise on Materials Science and Technology, Vol. 12, Glass I: Interaction with Electromagnetic Radiation, Tomozawa, M., and Doremus, R.H., eds., Academic, N.Y., 1977, 223.

35. Kumeda, M., Kobayashi, N., Suzuki, M., and Shimizu, T., ESR studies of Mn^{2+} in multicomponent amorphous semiconductors, Jpn. J. Appl. Phys., 14, 173, 1975.

36. Watanabe, I., Inagaki, Y., and Shimizu, T., ESR study of Mn^{2+} in Ge-Te and Ge-Te-Si glasses. J. Non-Cryst. Solids, 17, 109, 1975.

37. Miller, D.J., and Haneman, D., Effect of gas exposure in the EPR signal for amorphous silicon films, Solid State Commun, 27, 91, 1978.

38. Street, R.A., and Knights, J.C., Oxidatior and interface states in a-Si:H, Philos. Mag., B43, 1091, 1981.

39. Pontuschka, W.M., Carlos, W.E., and Taylor, P.C., Radiation-induced paramagnetism in a-Si:H, Phys. Rev., B25, 4362, 1982.

40. Ching, W.Y., Oxygen impurity states in an amorphous silicon matrix, Phys. Rev., B22, 2016, 1980; Laughlin, R.B., Joannopoulos, J.D., and Chadi, D.J., Electronic states of the Si-SiO_2 interface, in The Physics

23. Thomas, P.A., Brodsky, M.H., Kaplan, D., and Levine, D., Electron spin resonance of ultrahigh vacuum evaporated amorphous silicon. Insitu and exsitu studies, Phys. Rev., B18, 3059, 1978.

24. Fritzsche, H., and Hudgens, S.J., Magnetic properties of amorphous semiconductors, in Electronic Phenomena in Non-Crystalline Semiconductors, B.T. Kolomiets, eds., Nauka, Leningrad, USSR, 1975, 6.

25. Pawlik, J.R., Connell, G.A.N., and Prober, D., Magnetic proeprties of amorphous $Ge_{1-x}H_x$ and $Si_{1-x}H_x$ films, in Electronic Phenomena in Non-Crystalline Semiconductors, B.T. Kolomiets, ed., Nauka, Leningrad, USSR, 1975, 304.

26. Brodsky, M.H., and Title, R.S., Clues to the nature of the spin centers in amorphous silicon, in Structure and Excitations of Amorphous Solids, Lucovsky, G., and Galeener, F.L., eds., AIP Conference Proceedings, #31, AIP, New York, 1976, 97.

27. Hasegawa, S., and Imai, Y., Thickness dependence of electrical and optical properties and ESR in undoped a-Si:H, Philos. Mag., B46, 239, 1982.

28. Knights, J.C., Biegelsen, D.K., and Solomon, I., Optically induced electron spin resonance in doped amorphous silicon, Solid State Commun., 22, 133, 1977.

29. Di Salvo, F.J., Bagley, B.G., Tauc, J., and Waszxzak, J.V., Magnetic susceptibility of $CdGeAs_2$ in the polycrystalline, glassy and liquid states, in Amorphous and Liquid Semiconductors, Proc. Int. Conf., 5th, Stuke, J., and Brenig, W., eds., Taylor and Francis, London, 1974, 1043.

30. Taylor, P.C., Friebele, E.J. and Bishop, S.G., The effects of impurities on the paramagnetic gap states in amorphous As_2Se_3, in Physics of Semiconductors 1978, Wilson, B.L.H., ed., Institute of Physics Conf. Series, no. 43, Institute of Physics, London, 1979, 1305.

11. Bagley, B.G., Di Salvo, F.J., and Waszczak, J.V., The low temperature magnetic susceptibilities of crystalline and glassy sulfur and selenium, Solid State Commun., 11, 89, 1972.

12. Taylor, P.C., Baugher, J.F., and Kriz, H.M., Magnetic resonance spectra in polycrystalline solids, Chem. Revs., 75, 203, 1975.

13. Mott, N.F., Electrons in disordered structures, Advan. Phys., 16, 49, 1967.

14. Cohen, M.H., Fritzsche, H., and Ovshinsky, S.R., Simple band model for amorphous semiconducting alloys, Phys. Rev. Lett., 22, 1065, 1969.

15. Anderson, P.W., Model for the electronic structure of amorphous semiconductors, Phys. Rev. Lett., 34, 953, 1975.

16. Street, R.A. and Mott, N.F., States in the gap in glassy semiconductors, Phys. Rev. Lett., 35, 1293, 1975.

17. Mott, N.F., Davis, E.A., and Street, R.A., States in the gap and recombination in amorphous semiconductors, Philos. Mag., 32, 961, 1975.

18. Kastner, M., Adler, D., and Fritzsche, H., Valence-alternation model for localized gap states in lone pair semiconductors, Phys. Rev. Lett., 37, 1504, 1976.

19. Gubser, D.U., and Taylor, P.C., Low temperature magnetic susceptibility of vitreous As_2Se_3, Phys. Lett., 40A, 3, 1972.

20. Agarwal, S.C., Nature of localized states in amorphous semiconductors--a study by electron spin resonance, Phys. Rev., B7, 685, 1973.

21. Bishop, S.G., Strom, U., and Taylor, P.C., Optically induced metastable states in amorphous semiconductors, Phys. Rev., B15, 2278, 1977.

22. Hasegawa S., Yazaki, S., and Shimizu, T., Ferromagnetic interaction between spins in amorphous Si-Ge films, Solid State Commun., 23, 901, 1977

References

1. Di Salvo, F.J., Menth, A., Waszczak, J.V., and Tauc, J., Magnetic susceptibility of amorphous semiconductors, Phys. Rev., B15, 4574, 1972.
2. Tauc, J., and Menth, A., States in the gap, J. Non-Cryst. Solids, 819, 569, 1972.
3. Tauc, J. Menth, A., and Wood, D.L., Optical and magnetic investigations of localized states in semiconducting glasses, Phys. Rev. Lett., 25, 749, 1970.
4. Cimpl. Z., Kosek, F. and Matyas, M., Magnetic properties of As_2S_x glasses, Phys. Stat. Sol., 41, 535, 1970.
5. White, R.M., and Anderson, P.W., Magnetic properties of amorphous semiconductors I. Diamagnetic enhancement, Philos. Mag., 25, 737, 1972.
6. Busch, G., and Vogt, O., Magnetische Suszeptibilität vom flüssigen selen und tellur, Helv. Phys. Acta, 30, 224, 1957.
7. Červinka, L., Hrubý, A., Höschl, P. Matyáš, M., Šimeček, T. Škácha, J., Stouvac, L., Tauc, J., and Vorlíček, V., The structure and electronic properties of semiconducting glasses based on $CdAs_2$, J. Non-Cryst. Solids, 4, 258, 1970.
8. Matyáš, M., Magnetic properties of crystalline and amorphous $CdAs_2$, Phys. Status Solidi, 43, K63, 1971.
9. Matyáš, M., Magnetic Susceptibility of liquid semiconductors, Czech. J. Phys. B21, 992 (1971).
10. Novoselov, S.K., Strakhov, L.P. and Baidakov, L.A., Temperature dependence of the magnetic susceptibility of As_2Se_3 at the crystal-melt and glass-melt phase transitions, Sov. Phys. Solid State, 11, 1266, 1969.

spins. This information helps to characterize such paramagnetic sites as defects, impurities and localized electronic states which exist near the band edges as a result of local strains.

Nuclear paramagnetism provides a useful probe of local structural order of the major constituent atoms in amorphous semiconductors. The most important information obtained from nuclear magnetic resonance (NMR) measurements in these solids includes symmetries at bonding sites, inhomogeneities, local motion of atomic species and photo-induced changes in local structural order.

Both nuclear and electronic spin-lattice relaxation mechanisms are important probes of the electronic and vibrational properties in amorphous semiconductors. ESR and NMR measurements have indicated, at least indirectly, the presence of low frequency, anharmonic tunneling modes in most chalcogenide, pnictide and tetrahedral amorphous semiconductors. In some materials spin-lattice relaxation also probes important defects and impurities such as dangling bonds or trapped molecular species.

Ackowledgments

Mary Woolf and Vince Frederick are gratefully acknowledged for invaluable help with the preparation of the manuscript. Portions of the research described in this chapter were supported by the National Science Foundation under grant number DMR-83-04471 and by the Office of Naval Research.

In the ODMR technique optical excitation is applied in the presence of a magnetic field, and a photoluminescence (PL) or absorption signal is monitored. Either as the result of the thermalization of electrons and holes or as a consequence of different decay rates for different magnetic sub-levels, one observes differences in strongly emitting states as a function of the magnetic field.

The major conclusions from ODMR experiments in the chalcogenide glasses are that there may be more than one PL band and that triplet states may exist in these glasses. In a-Si:H and related alloys the ODMR results are quite complicated, but they do tend both to support and to supplement the existing models for the PL processes in these films.

VII. SUMMARY

Our understanding of the basic structural and electronic properties of amorphous semiconductors has been greatly aided by investigations of magnetic effects in these materials. Most chalcogenide glasses are diamagnetic under equilibrium conditions, but the pnictide and tetrahedrally-bonded amorphous semiconductors often exhibit a paramagnetism which is usually attributed to unsatisfied bonds. In the chalcogenide glasses there is a slight tendency to be more diamagnetic than corresponding crystalline forms.

Although the chalcogenide glasses are diamagnetic, there is a metastable, optically-induced paramagnetism which exists at low temperatures. In a-Si:H and related alloys both transient and metastable contributions to optically-induced paramagnetism exist with some of the metastable component existing up to ~ 400K.

Electron spin resonance (ESR) measurements in amorphous semiconductors often yield detailed local descriptions of the wave functions of the unpaired

There have been few, if any, Mössbauer studies of the tetrahedral amorphous semicondcutors, but the technique has been used effectively for the chalcogenide glasses. The most studied nucleus is ^{125}Te but ^{119}Sn and ^{121}Sb have also been used as probes.

The electric and magnetic hyperfine interactions have been utilized in films of amorphous Te, in Se doped with Te and in $GeSe_1Te_{1-x}$ to investigate the structure of these materials.[151-154] As in the case of NMR, amorphous Te is found to contain a distribution of quadrupolar interactions[151] with the average quadrupolar coupling constant slightly larger than in the crystalline phase. This increase has been attributed[152] to an increase in the first nearest neighbor distance in the amorphous film.

In glassy Te-doped Se the observed quadrupolar splittings are intermediate between those observed in the trigonal and monoclinic crystals of Se. This result suggests that both the monoclinic rings and the trigonal chains exist in glassy Se[153] although the average bonding properties are closer to those in monoclinic Se.[155] Recently ^{125}Te and ^{129}I Mössbauer investigations of Ge_xSe_{1-x} and GeS_2 glasses have discovered at least two distinct sites[156,157] which suggest that there is substantial intermediate range order in these glasses.

VI. ODMR

Magnetic effects in amorphous semiconductors can also be probed by optical techniques. Although it is not the primary focus of this chapter, this section summarizes some of the important aspects of these optical approaches. Recent reviews of optically detected magnetic resonance (ODMR) in the tetrahedral amorphous semiconductors[158,159] and the chalcogenide glasses[159] are available.

not serve as a relaxation center. The coupling of the molecular hydrogen to the lattice yields the minimum in T_1.

The most important test of this model is to look for the conversion of the orthohydrogen to parahydrogen which is a slow bimolecular process at low temperatures. Figure 26 shows that indeed the T_1 minimum value does increase with the time during which the sample is kept at low temperatures. The increase shown in Fig. 26 is consistent with the expected bimolecular kinetics. Although some minor difficulties reamin,[112] these low temperature annealing experiments provide firm evidence for the presence of H_2 molecules in a-Si:H films made by the glow-discharge technique.

Recently several experiments, including ^1H NMR measurements,[150] have indicated that the T_1 results probe only some of the trapped H_2 in films of a-Si:H. In at least some films there can be an order of magnitude more molecular hydrogen (~ 1 at.% of the atoms in the film) than that which contributes to the T_1 minmum.

V. MÖSSBAUER SPECTROSCOPY

The Hamiltonian in Mössbauer spectroscopy contains terms similar to those which appear in NMR except that differences between an excited state and the ground state of the nucleus are probed using this technique. In Mössbauer spectroscopy the analogs of the Zeeman, quadrupolar and chemical shift interactions are the magnetic hyperfine, electric hyperfine and isomer shift interactions, respectively. In the harmonic approximation the probability of observing a Mössbauer transition f' is proporitonal to an exponential which contains a scalar product of a nuclear vibrational amplitude vector and the directional vector for the incident gamma ray.

The model interpretations[116,144,145] of these low temperature T_1 data all involve coupling to "tunneling" modes or "disorder" modes. In this model the elementary excitations consist of ordinary phonons and a series of two-level (highly anharmonic) systems often called disorder modes. The ensemble of disorder modes exhibits a continuous distribution of energy splittings where in each case the two levels are separated by a relatively high potential barrier. The physical origin of these modes is considered to be atoms or groups of atoms which can sit in two nearly equivalent, metastable equilibrium positions. The exact process by which the nuclear spins are relaxed continues to be a matter of some debate.[144,145]

2. Defects and Impurities

Several authors[112,129,142,147,148] have studied the spin-lattice relaxation of ^1H in a-Si:H over a temperature range from ~ 4 to ~ 800K. Below 300K there exists a characteristic minimum in T_1 as a function of T. This miminum, which occurs near 30K, is found in nearly all films studied to date. Typical data are shown in Fig. 25. At temperatures above the minimum in T_1 the data are independent of frequency, but at low temperatures there exists a weak temperature dependence.[112] Some sputtered samples, which are deliberately made with a low hydrogen content, do not exhibit this minimum (see Fig. 25). In these films the spin-lattice relaxation is thought to be due to the paramagnetic silicon dangling bonds.[147]

Conradi and Norberg[149] have suggested that trapped molecular hydrogen molecules act as the relaxation centers while the rest of the (bonded) hydrogen is relaxed by spin diffusion to these centers. Molecular hydrogen can exist in two spin states, ortho (I = 1) and para (I = 0), whose relative densities vary with the temperature once thermal equilibrium has been established. At low temperatures the orthohydrogen gradually converts to parahydrogen which does

action of Eq. (11)) by a Raman process involving either phonons or some other lattice modes. In crystalline solids the low temperature behavior of T_1 results from first-order Raman phonon processes which yield rapid temperature dependences ($T_1 \propto T^{-7}$ or T^{-9}). In amorphous solids the low temperature spin lattice relaxation rates are always faster than in corresponding crystalline solids, and the temperature dependences obey much weaker power laws.[143] Data for As_2S_3, and As are shown in Fig. 24.

Table 3 lists[116,121,124,144,145] the observed exponents β in the power law behavior for $T_1(T_1 \propto T^{-\beta})$ for most of the amorphous solids which have been investigated. It is apparent from Table 3 that β falls in the range $1 < \beta < 2$. The last two entries indicate that these results are not restricted to quadrupolar nuclei because the spins of ^{31}P, ^{203}Tl and ^{205}Tl are I = 1/2. In addition Haupt and Müller-Warmuth[145] have obtained values of β between 1.5 and 2 for hydrogen (I = 1/2) in various organic glasses. In these cases the relaxation presumably proceeds via a modulation of the dipolar or chemical shift interactions by a Raman process involving low energy excitations. The Raman process should be essentially frequency independent, a fact which is confirmed in those cases where the frequency can be varied (last four entries of Table 3 which involve NMR experiments). The data on $Tl_2SeAs_2Te_3$ indicate that the relaxation is independent of the nuclear isotope. The low temperature regime over which the power law behavior holds varies from material to material, but this range extends to at least 200 K in all cases.

Of the pnictide and chalcogenide amorphous semiconductors studied to date only amorphous P (a-P) fails to follow the pattern shown in Table 3. In a-P where the relaxation times are long and essentially temperature independent, the relaxation is thought to be due to the presence of paramagnetic impurities.[124]

case of hydrogen. The results indicate that, like the hydrogen atoms, the boron atoms are clustered in a-Si:H,B. Although clustering is definitely present, it is not sufficient to produce many B-B bonds.

Phosphorus doping in a-Si:H films has also been examined using NMR techniques[141] where different P bonding environments can be inferred from the chemical shift interaction (Eq. (10)). At least two NMR lines are observed which are centered at different frequencies (different chemical shifts). One line is attributed to threefold-coordinated phosphorus and the other to fourfold-coordinated phosphorus,[141] and the ratio of three- to four-coordinated sites is about 4 to 1.

A final use of NMR techniques to determine local structural properties in a-Si:H and related alloys is to monitor hydrogen diffusion and evolution. In films with the lowest defect densities (see Section III.A.2), the clustered hydrogen (broad ^1H NMR line) is the first species to evolve.[129,142] As the hydrogen goes off, an increase in the ESR occurs.

B. Spin-Lattice Relaxation

Nuclear spin systems can relax via the lattice in a fashion analogous to that described in section III.E for electronic spin systems. The characteristic time for this relaxation to occur is also denoted as T_1 for the case of nuclear spins. In the chalcogenide and pnictide amorphous semiconductors, T_1 measurements have provided a probe, albeit indirect, of anharmonic, low frequency tunneling or disorder modes. In a-Si:H and related alloys spin-lattice relaxation occurs either via trapped molecular hydrogen (H_2) or by paramagnetic defects (dangling bonds).

1. Low Frequency Lattice Modes

For nuclei of spin $I > 1/2$ the nuclear spin-lattice relaxation usually results from the modulation of the electric field gradient (quadrupolar inter-

NMR studies of those silicon atoms which possess a nuclear spin (5%) have yielded ambiguous results, primarily because the signals are weak and the lines are broad and poorly resolved. Because the spin of ^{29}Si is 1/2 only the chemical shift (Eq. (10)) and dipolar (Eq. (6)) interactions are important. Unlike the case of hydrogen the results depend dramatically on the samples which are studied.[127,133-135] There is general agreement that the chemical shift increases as one adds SiH_2 and SiH_3 groups to the films, but the absolute shifts appear to vary from film to film. The reason for these variations is probably that the silicon bonds are distorted in a-Si:H and these distortions vary with sample preparation.

There have also been some NMR investigations of dopants in a-Si:H films and alloys. In the case of boron (p-doping), ^{11}B NMR experiments[136,137,138] provide an explanation of the low doping efficiency in a-Si:H. A typical ^{11}B NMR lineshape is shown in Fig. 23. This lineshape indicates that all the observable boron ($\gtrsim$ 99%) is three coordinated and therefore unlikely to be a dopant. This conclusion comes from the quadrupolar term in the Hamiltonian (Eq. (11)) which is very sensitive to local bonding symmetry.

Two lines are observed in the ^{11}B NMR from a film with $\sim$ 10 at.% B (see Fig. 23). Greenbaum et al.[136] suggest that the broad and narrow lines in Fig. 23 result from planar, three-coordinated boron atoms in BSi_3 and Si_2BH configurations, respectively. In films with less than 1 at.% boron the broad line is absent[137,138] which suggests that essentially all of the boron is bonded to at least one hydrogen in these films. This conclusion in turn implies that the hydrogen must be preferentially bonded to the boron which is precisely the conclusion drawn from infrared absorption measurements.[139,140]

The dipolar interaction between boron nuclei can be used to estimate the average boron-boron separation in a-Si:H,B films[136,137] just as it was for the

60. Kumeda, M., Jinno, Y., Watanabe, I., and Shimizu, T., Electron spin resonance in amorphous Si and Ge doped with Mn, Solid State Commun., 23, 833, 1977.

61. Biegelsen, D.K., Street, R.A., Tsai, C.C., and Knights, J.C., Defect creation and hydrogen evolution in amorphous Si:H, J. Non-Cryst. Solids, 35 + 36, 285, 1980.

62. Hasegawa, S., and Imai, Y., Annealing effects on relationships between ESR, electrical and optical properties in a-Si:H, Philos. Mag., B45, 347, 1982.

63. Kumeda, M., and Shimizu, T., ESR in hydrogenated amorphous silicon, Jpn, J. Appl. Phys., 19, L197, 1980.

64. Biegelsen, D.K., Electron spin resonance studies of amorphous silicon, Proc. Electron Resonance Soc. Symp., 3, 85, 1981.

65. Ishii, N., Kumeda, M., and Shimizu, T., The effects of H and F on the ESR in a-Si, Jpn. J. Appl. Phys., 21, L92, 1982.

66. Adler, D., Electronic properties of amorphous silicon alloys, Kinam, C4, 225, 1982.

67. Adler, D., and Frye, R.C., Electronic structure of amorphous silicon alloys, AIP Conf. Proc., 73, 146, 1981.

68. Adler, D., and Shapiro, F.R., Effective correlation energy of the dangling bond in amorphous silicon, Physica 117B + 118B, 932, 1983.

69. Stuke, J., ESR in amorphous germanium and silicon, in Amorphous and Liquid Semiconductors, Spear, W.E., ed., University of Edinburgh, Edinburgh, Scotland, 1977, 406.

70. Hasegawa, S., Kasajima, T., and Shimizu, T., Doping and annealing effects on ESR in chemically vapor deposited amorphous silicon, Solid State, Commun. 29, 13, 1979.

71. Hasegawa, S., Shimizu, T., and Hirose, M., ESR in heavily doped CVD amorphous silicon films, J. Phys. Soc. Jpn., 49, Suppl. A, 1237, 1980.

72. Hasegawa, S., Kasajima, T., and Shimizu, T., ESR in doped CVD amorphous silicon films, Philos. Mag., B43, 149, 1981.

73. Street, R.A., Biegelsen, D.K., and Knights, J.C., Defect states in doped and compensated a-Si:H, Phys. Rev., B24, 969, 1981.

74. Dersch, H., Stuke, J., and Beichler, J., Electron spin resonance of doped glow-discharge amorphous silicon, Phys. Status Solidi, B105, 265, 1981.

75. Margarino, J., Kaplan, D., Friederich, A., and Deneuville, A., Doping effects on post-hydrogenated chemical-vapor deposited amorphous silicon, Philos. Mag., B45, 285, 1982.

76. Dersch, H., Stuke, J., and Beichler, J., Temperature dependence of ESR spectra, Phys. Status Solidi, B107, 307, 1981.

77. Overhof, H., and Beyer, W., Density of states in amorphous Si:H, Phys. Status Solidi, B107, 207, 1981.

78. Overhof, H., Temperature dependence of the spin resonance in boron doped a-Si:H, Phys. Status Solidi, B110, 521, 1982.

79. Biegelsen, D.K., Street, R.A., and Knights, J.C., Auto compensation in doped amorphous silicon, AIP Conf. Proc., 73, 166, 1981.

80. Fischer, R., Rehm, W., Stuke, J., and Voget-Grote, U., Thermalization and recombination of excess carriers in a-Si:H, J. Non-Cryst. Solids, 35 + 36, 687, 1980.

81. Bishop, S.G., Strom, U., and Taylor, P.C., Optically induced localized paramagnetic states in chalcogenide glasses, Phys. Rev. Lett 34, 346, 1975; Optically induced localized paramagnetic states in amorphous semiconductors, Phys. Rev. Lett, 36, 543, 1976.

82. Taylor, P.C., Strom, U., and Bishop, S.G., Temperature dependence of the density of optically-induced localized paramagnetic states in glassy As_2Se_3, Philos. Mag., B37, 241, 1978.

83. Bishop, S.G., Strom, U., Friebele, E.J., and Taylor, P.C., The effects of impurities upon photoluminescence and optically induced paramagnetic states in chalcogenide glasses, J. Non-Cryst. Solids, 32, 359, 1979.

84. Gaczi, P.J., As and S centered paramagnetic species in sulphide glasses, Philos. Mag., B45, 241, 1982; Pontuschka, W.M., and Taylor, P.C., ESR in x-irradiated As_2O_3 glass, Solid State Commun., 38, 573, 1981.

85. Bishop, S.G., Strom, U., and Taylor, P.C., Localized electronic states in glassy Se, in The Physics of Selenium and Tellurium, Gerlach, E., and Grosse, P., eds., Springer-Verlag, New York, 1979, 193.

86. Arai, K., and Namikawa, H., ESR in Ge-S glass, Solid State Commun. 13, 1167, 1973.

87. Černý, V., and Frumar, M., ESR study and model of paramagnetic defects in Ge-S glasses, J. Non-Cryst. Solids, 33, 23, 1979.

88. Watanabe, I., Ishikawa, M., and Shimizu, T., On the property and origin of paramagnetic defects in amorphous Ge-S and Ge-S-Ag, J. Phys. Soc. Jpn., 45, 1603, 1978.

89. Watanabe, I., Shiomi, S., and Shimizu, T., Effective electron correlation energy in amorphous Ge-S, J. Phys. Soc. Jpn., 51, 2525, 1982.

90. Benoit á la Guillaume, C., Mollot, F., and Cernogora,J., About photo-induced centres in amorphous chalcogenide semiconductors, in Amorphous and Liquid Semiconductors, Spear, W.E., ed., University of Edinburgh, Edinburgh, Scotland, 1977, 612.

91. Biegelsen, D.K. and Street, R.A., Photo induced defects in chalcogenide glasses, Phys. Rev. Lett., 44, 803, 1980.

92. Bishop, S.G., Strom, U., and Taylor, P.C., Optically induced localized paramagnetic states in amorphous As, Solid State Commun., 18, 573, 1976.

93. Taylor, P.C., Friebele, E.J., and Bishop, S.G., Thermally generated paramagnetism in amorphous arsenic, Solid State Commun., 28, 247, 1978.

94. Shanabrook, B.V., Bishop, S.G. and Taylor, P.C., Photoluminescence and ESR studies of localized states in amorphous phosphorus, J. de Phys., Colloq. C4, 42, 865, 1981.

95. Shanabrook, B.V., and Taylor, P.C., Optically and x-ray induced paramagnetism in amorphous phosphorus, Phys. Rev., B28, 1239, 1983.

96. Emin, D., Seager, C.H., and Quinn, R.K., Small-polaron hopping motion in some chalcogenide glasses, Phys. Rev. Lett., 28, 813, 1972.

97. Emin, D., Small-polaron model of the low-temperature optically induced properties of chalcogenide glasses, in Amorphous and Liquid Semiconductors, Spear, W.E., ed., University of Edinburgh, Edinburgh, Scotland, 1977, 261.

98. Pawlik, J.R., and Paul, W. EPR and photo-EPR in doped and undoped amorphous Si and Ge, in Amorphous and Liquid Semiconductors, Spear, W.E., ed., University of Edinburgh, Edinburgh, Scotland, 1977, 437.

99. Friederich, A. and Kaplan, D., Light-induced E.S.R. in amorphous silicon, J. Electron. Mater. 8, 79, 1979.

100. Street, R.A. and Biegelsen, D.K., Explanation of light induced ESR in a-Si:H; Dangling bonds with a positive correlation energy, J. Non-Cryst. Solids, 35 + 36, 651, 1980.

101. Biegelsen, D.K., Street, R.A., and Jackson, W.B., Distribution of recombination lifetimes in doped a-Si:H, Physica, 117B + 118B, 899, 1983.

102. Street, R.A., and Biegelsen, D.K., Distribution of recombination lifetimes in amorphous silicon, Solid State Commun., 44, 501, 1982.

103. Boulitrop, F., and Dunstan, D.J., Non-geminate recombination in amorphous silicon, a study by light-induced ESR, Solid State Commun., 44, 841, 1982.

104. Friederich, A., and Kaplan, D., Doping effects in CVD deposited amorphous silicon, J. Phys. Soc. Jpn., Suppl. A, 49, 1233, 1980.

105. Taylor, P.C., and Ohlsen, W.D., Optical instabilities and localized electronic states in hydrogenated amorphous silicon, Solar Cells, 9, 113, 1983.

106. Lee, C., Ohlsen, W.D., Taylor, P.C., Ullal, H.S., and Ceasar, G.P., Dependence of the metastable light-induced ESR in a-Si:H on temperature and power, AIP Conf. Proc., 120, 205, 1984.

107. Stutzmann, M., Jackson, W.B., and Tsai, C.C., The kinetics of formation and annealing of light-induced defects in hydrogenated amorphous silicon, AIP Conf. Proc., 120, 213, 1984.

108. Lee, C., Ohlsen, W.D., and Taylor, P.C., Kinetics of the metastable optically-induced ESR in a-Si:H, Phys. Rev., B31, 100, 1985.

109. Gourdon, J.C., Fretier, P., and Pescia, J., Spin-lattice relaxation in amorphous silicon. Evidence of anomalous temperature dependences, J. Phy. Lett., Orsay, 42, 21, 1981.

110. Movaghar, B., Overhof, H., and Schweitzer, L., ESR and spin-relaxation in amorphous germanium and silicon, in Amorphous and Liquid Semiconductors, Spear, W.E., ed., University of Edinburgh, Edinburgh, Scotland, 1977, 419.

111. Stutzmann, M., and Biegelsen, D.K., Electron-spin-lattice relaxation in amorphous silicon and germanium, Phys. Rev., B28, 6256, 1983.

112. Carlos, W.E., and Taylor, P.C., ^{1}H NMR in a-Si, Phys. Rev. B26, 3605, 1982.

113. Bishop, S.G., and Taylor, P.C., Atomic reorientation rates in liquid chalcogenide glasses, Solid State Commun., 11, 1323, 1972.

114. Bishop, S.G., and Taylor, P.C., Correlation times for local structural order in liquid semiconductor glasses: NMR in Se and As_2Se_3, Proc. 11th Int. Conf. on Physics of Semicond., Warsaw, Poland, 1972, 576.

115. Bishop, S.G., and Taylor, P.C., Nuclear-magnetic resonance studies of bonding in semiconducting Tl-As-Se glasses, Phys. Rev., B7, 5177, 1973.

116. Rubinstein, M., and Taylor, P.C., Nuclear quadrupole resonance in amorphous and crystalline As_2S_3, Phys. Rev., B9, 4258, 1974.

117. Taylor, P.C., Strom, U., Pontuschka, W.M., and Treacy, D.J., Nuclear quadrupole resonance probes of structural and photostructural properties of glassy As_2Se_3, As_2S_3 and As_2O_3, J. Phys. Soc. Jpn., 49, Suppl. A, 1155, 1980.

118. Szeftel, J., and Alloul, H., Study of the local structure in vitreous chalcogenides via measurement of the asymmetry of the electric-field-gradient tensor, Phys. Rev. Lett., 42, 1691, 1979.

119. Szeftel, J., Local symmetry and chemical characteristics of the arsenic site in As containing glasses, Philos. Mag., B43, 549, 1981.

120. Treacy, D.J., Strom, U., Klein, P.B., Taylor, P.C., and Martin, T.P., Photostructural effects in glassy As_2Se_3 and As_2S_3, J. Non-Cryst. Solids, 35 + 36, 1035, 1980; Treacy, D.J., Taylor, P.C. and Klein, P.B., Photodarkening and photostructural effects in glassy As_2Se_3, Solid State Commun., 32, 423, 1979.

121. Jellison, G.E., Jr., Petersen, G.L., and Taylor, P.C., Nuclear quadrupole resonance studies of amorphous, orthorhombic, and rhombohedral arsenic, Phys. Rev., B22, 3903, 1980.

122. Petersen, G.L., Jellison, G.E., Jr., and Taylor, P.C., Pulsed NQR in amorphous, orthorhombic and rhombohedral arsenic, J. Molec. Structure, 58, 263, 1980.

123. Greaves, G.N., and Davis, E.A., A continuous random network model with three-fold coordination, Philos. Mag., 29, 1201, 1974.

124. Jellison, G.E., Jr., NMR studies of amorphous phosphorus, Solid State Commun., 30, 481, 1979.

125. Reimer, J.A., Vaughan, R.W. and Knights, J.C., Proton magnetic resonance spectra of plasma-deposited amorphous Si:H films, Phys. Rev. Letters, 44, 193, 1980.

126. Carlos, W.E., and Taylor, P.C., Hydrogen-associated disorder modes in amorphous Si:H films, Phys. Rev. Lett., 45, 358 (1980).

127. Jeffrey, F.R., and Lowry, M.E., Determination of the H distribution in reactively sputtered amorphous silicon-hydrogen alloys by proton nuclear magnetic resonance, J. Appl. Phys., 52, 5529, 1981.

128. Kumeda, M., Yonezawa, Y., Nakazawa, K., Ueda, S., and Shimizu, T., Hydrogen incorporation scheme in amorphous-microcrystalline mixed-phase hydrogenated silicon films, Jpn. J. Appl. Phys., 22, L194, 1983.

129. Reimer, J.A., Vaughan, R.W., and Knights, J.C., Proton-magnetic-resonance studies of microstructure in plasma-deposited amorphous-silicon-hydrogen films, Phys. Rev., B24, 3360, 1981.

130. Jeffrey, F.R., Murphy, P.D., and Gerstein, B.C., ^{29}Si NMR spectra for reactively sputtered amorphous silicon, Phys. Rev., B23, 2099, 1981.

131. Leopold, D.J., Boyce, J.B., Fedders, P.A., and Norberg, R.E., Deuteron and proton magnetic resonance in a-Si:H(D,H), Phys. Rev., B26, 6053, 1982.

132. Norberg, R.E., 1985, private communication.

133. Lamotte, B., Rousseau, A., and Chenevas-Paule, A., High resolution NMR of ^{29}Si in amorphous hydrogenated silicon, J. Phys. Colloq., 42-C4, 839, 1981.

134. Shanks, H.R., Jeffrey, F.R., and Lowry, M.E., Bonding in hydrogenated amorphous silicon, J. Phys. Colloq., 42-C4, 773, 1981.

135. Reimer, J.A., Murphy, P.D., Gerstein, B.C., and Knights, J.C., Silicon-29 corss-polarization magic-angle sample spinning spectra in amorphous silicon-hydrogen films, J. Chem. Phys., 74, 1501, 1981.

136. Greenbaum, S.G., Carlos, W.E., and Taylor, P.C., The coordination of boron in a-SI:(B,H), Solid State Commun., 43, 663, 1982.

137. Greenbaum, S.G., Carlos, W.E., and Taylor, P.C., Boron and hydrogen bonding in B-doped a-Si:H--an NMR study, Physica, 117B + 118B, 886, 1983.

138. Greenbaum, S.G., Carlos, W.E., and Taylor, P.C., Local bonding arrangements of boron in doped hydrogenated amorphous silicon, J. Appl. Phys., 56, 1874, 1984.

139. Shen, S.C., and Cordona, M., Infrared and far-infrared absorption of B- and P-doped amorphous Si, Phys. Rev. B23, 5322, 1981.

140. Tsai, C.C., Characterization of amorphous semiconducting silicon-boron alloys prepared by plasma decomposition, Phys. Rev., B19, 2041, 1979.

141. Reimer, J.A., and Duncan, T.M., Local bonding configuration of phosphorus in doped and compensated hydrogenated amorphous silicon, Phys. Rev., B27, 4895, 1983.

142. Carlos, W.E., and Taylor, P.C., High temperature ^{1}H NMR in a-Si:H, J. Phys. Colloq., 42-C4, 725, 1981.

143. Taylor, P.C., Nuclear Spin Relaxation Phenomena in amorphous semiconductors, J. Non-Cryst. Solids, 59 + 60, 109, 1983.

144. Szeftel, J., and Alloul, H., Nuclear spin lattice relaxation in the amorphous state: towards an understanding, J. Non-Cryst. Solids, 29, 253, 1978.

145. Reinecke, T.L., and Ngai, K.L., Low-temperature nuclear-spin-lattice relaxation in glasses, Phys Rev., B12, 3476, 1975.

146. Haupt, J., and Müller-Warmuth, W., Kernrelaxation und quanteneffekte bei der methylgruppenrotation von festem toluol und toluolderivaten, Z. Naturforsch., 24a, 1066 (1969).

147. Carlos, W.E., Taylor, P.C., Oguz, S., and Paul, W., NMR studies of supttered and glow discharge deposited a-Si:H, AIP Conf. Proc., 73, 67, 1981.

148. Carlos, W.E., and Taylor, P.C., Molecular hydrogen in a-Si:H, Phys. Rev., B25, 1435, 1982.

149. Conradi, M.S., and Norberg, R.E., Molecular H_2: Nuclear spin relaxation centers in a-Si:H, Phys. Rev., B24, 2285, 1981.

150. Boyce, J.B., and Stutzmann, M., Orientational Ordering and melting of molecular H_2 in an a-Si matrix: NMR studies, unpublished.

151. Blum, N.A., and Feldman, C., Mössbauer study of amorphous and crystalline tellurium, Solid State Commun., 15, 965, 1974.

152. Boolchand, P., Triplett, B.B., Hanna, S.S., and de Neufville, J.P., in Mossbauer Effect Methodology, Graverman, I.J., Seidel, C.W., and Dieterly, D.K., eds., vol. 9, Plenum Press, N.Y., 1974, 53.

153. Boolchand, P., Amorphous and crystalline selenium--a Mössbauer effect study, Solid State Commun. 12, 753, 1973.

154. Henneberger, T., and Boolchand, P., Nuclear quadrupole interaction at Te^{125} in monoclinic selenium, Solid State Commun. 13, 1619, 1973.

155. Kim, C.S., and Boolchand, P., Chemical bonding in sulfur, selenium and tellerium from ^{129}I and ^{125}Te Mössbauer investigations, Phys. Rev., B19, 3187, 1979.

156. Bresser, W.J., Boolchand, P., Suranyi, P. and de Neufville, J.P., Intrinsically broken chalcogen chemical order in stoichiometric glasses, J. Phys. Colloq., 42-C4, 193, 1981.

157. Boolchand, P., Grothaus, J., and Phillips, J.C., Broken chemical order and phase separation in Ge_xSe_{1-x} glasses, Solid State Commun., 45, 183, 1983.

158. Morigaki, K., Optically detected magnetic resonance, in Semiconductors and Semimetals, Vol 21, Pankove, J.I., ed., Academic, N.Y., 1984, 155.

159. Cavenett, B.C., Optically detected magnetic resonance (O.D.M.R.) investigations of recombination processes in semiconductors, Adv. Phys. 30, 475, 1981.

Table 1

The Magnetic Susceptibility of Five Different Semiconductors in the Polycrystalline and Amorphous Phases in Units of 10^{-6} emu/gm (after reference 1)

Solid	Magnetic Susceptibility		Reference
	Polycrystalline	Glassy	
S	-.485	-.485	10
Se	-.272	-.291	10
$CdAs_2$	-.258	-.269	8
As_2S_3	-.345	-.355	1
As_2Se_3	-.287	-.292	1

Table 2

Saturated Densities of Optically Induced Paramagnetic Centers and Typical Inducing Photon Energies for Several Amorphous Semiconductors

Glass	Typical Inducing Energy (eV)	N_s (spins/cm^3)	Reference
Se	2.0	10^{16}	81
As_2Se_3	1.8	10^{17}	81
As_2S_3	2.4	10^{17}	81
As_2O_3	~ 5.0	10^{19}	84
$GeSe_2$	2.2	10^{16}	81
GeS_2	2.5	> 10^{17}	33
P	2.0	10^{17}	95
As	1.1	10^{17}	81

Table 3

Values of the Power Law Exponent β ($T_1 \propto T^{-\beta}$) for low-temperature spin-lattice relaxation in amorphous solids. (After ref. 143.)

Solid	Nucleus	β	Reference
As_2S_3	^{75}As	2.0	116
As_2Se_3	^{75}As	1.8	121
As	^{75}As	1.5	121
$(Na_2O)_{0.3}(SiO_2)_{0.7}$	^{23}Na	1.4	144
B_2O_3	^{11}B	1.3	144
Tl_2Se-$2As_2Se_3$	^{203}Tl,^{205}Tl	1.1	145
CaO-P_2O_5	^{31}P	1.0	124

Fig. 1. Magnetic susceptibility of As_2S_3 and As_2Se_3 glasses. (After ref. 1).

Fig. 2. Temperature dependent susceptibility, $\chi(T)$, for pure As_2Se_3 (solid circles) and As_2Se_3 + 10 ppm Fe (open circles). The data have been corrected for the magnetic background of the sample holder as indicated by the solid line through the pure As_2Se_3 data. (After ref. 19.)

Fig. 3. Characteristic ESR spectra for Fe^{3+} and Cu^{2+} impurities in glassy As_2Se_3.

Fig. 4. Intensity of the Fe^{3+} ESR response in glassy As_2Se_3 as a function of the amount of several intentionally-added impurities. The Fe is an inadvertent impurity in these samples and the valence state changes from predominantly 2+ to predominantly 3+ with the addition of most impurities (except iodine).

Fig. 5. ESR derivative spectra for two different samples of O-doped a-Si:H. The bottom traces are due to atomic hydrogen and are run under conditions to minmize the distortion in these line shapes due to excess microwave power and magnetic field modulation. The features near 3200 G are due to overlapping signals from the oxygen-related hole centers, the usual "dangling-bond" signal and silicon E' centers, but the line shapes are distorted. (After ref. 39.)

Fig. 6. ESR spectra at 30K in doped samples of a-Si:H. The top trace is heavily P-doped and the bottom trace is heavily B-doped. (After ref. 73.)

Fig. 7. Optically-induced ESR spectra obtained near 4.2K in several chalcogenide glasses. The dashed line superimposed on the Se spectrum is a computer simulation as described in the text. (After ref. 81.)

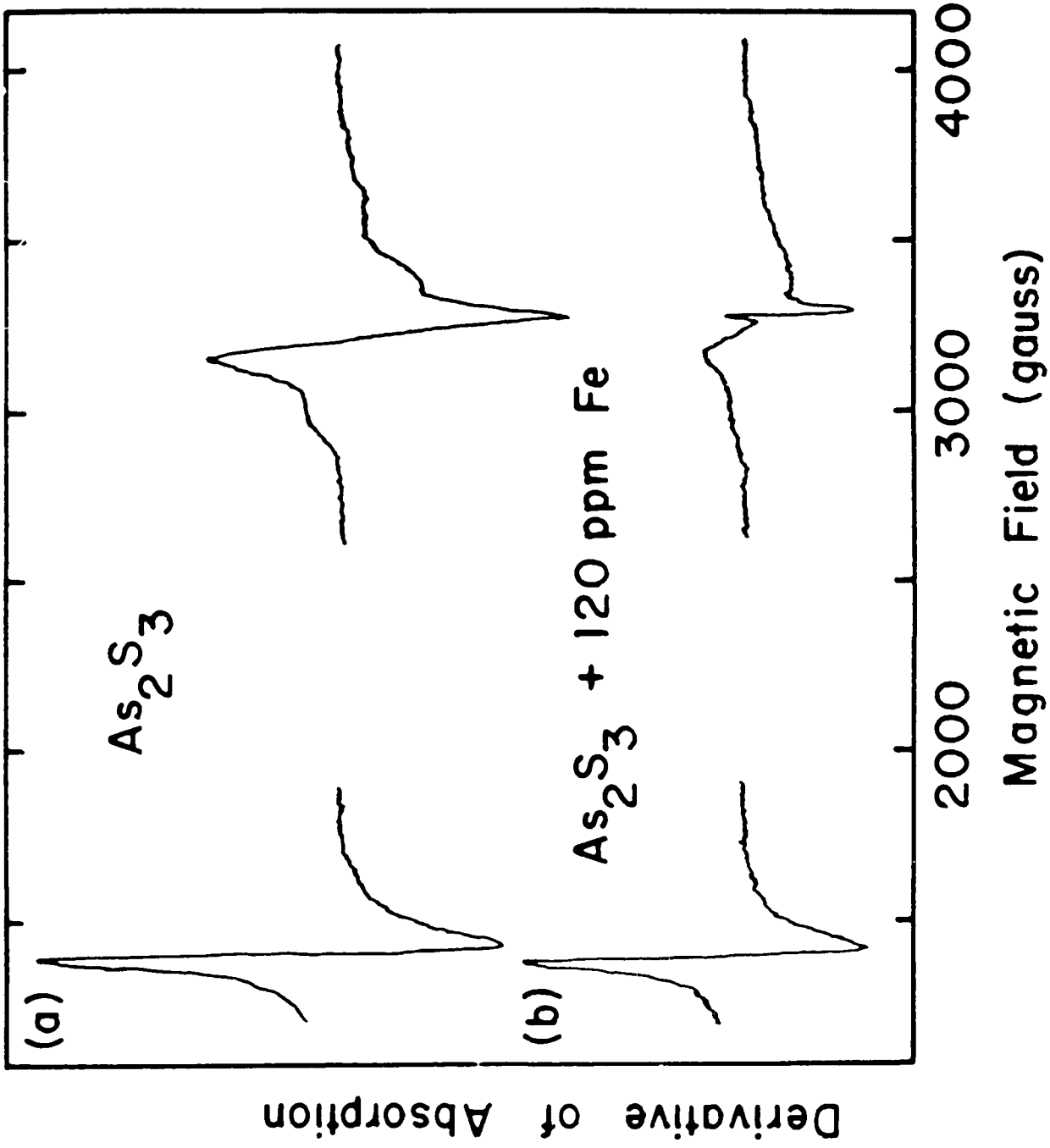
(a)
As_2S_3
(b)
As_2S_3 + 120 ppm Fe
2000
3000
4000
Magnetic Field (gauss)
Derivative of Absorption

Fig. 10

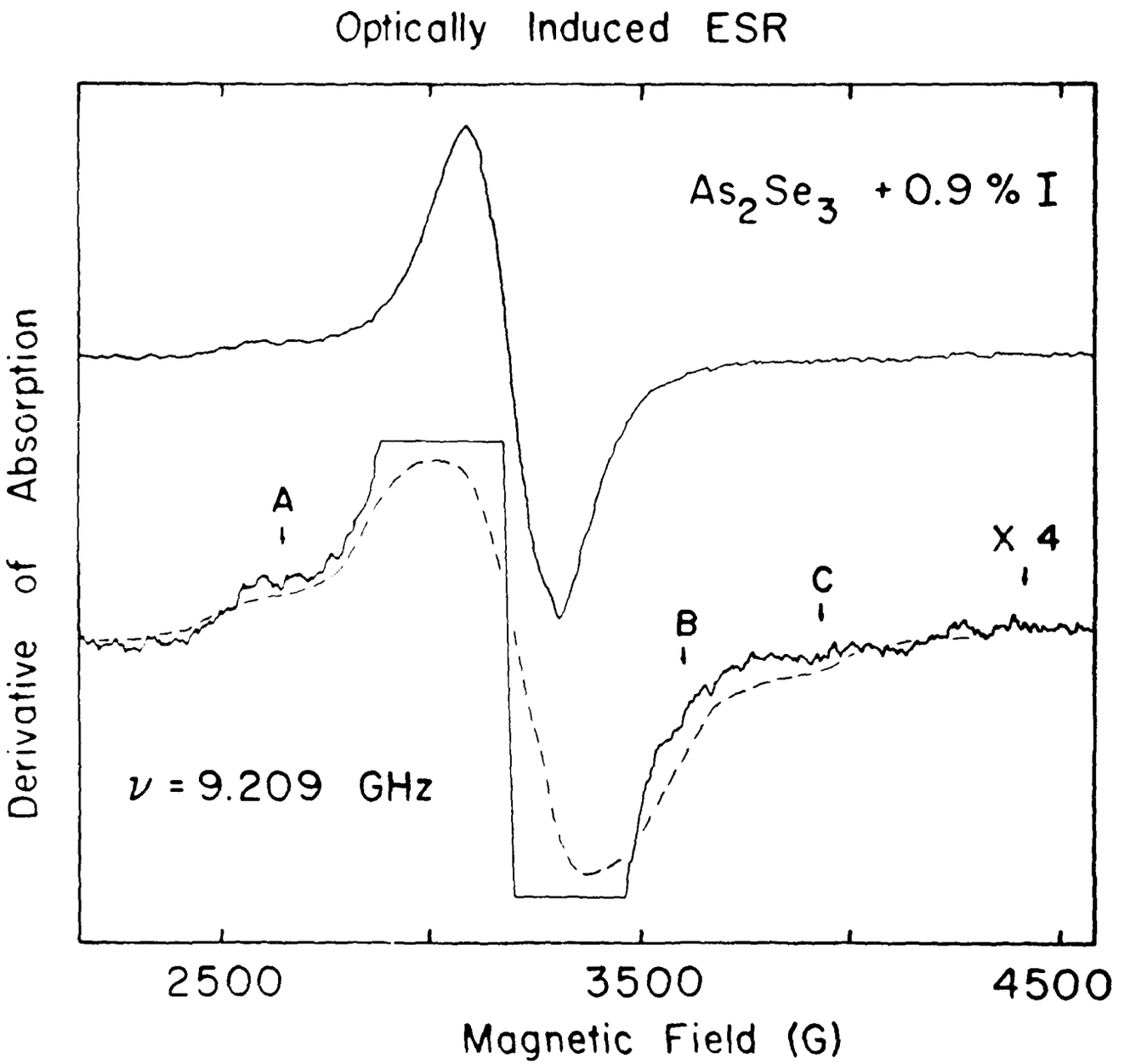

Fig. 9

P.C. Taylor 79

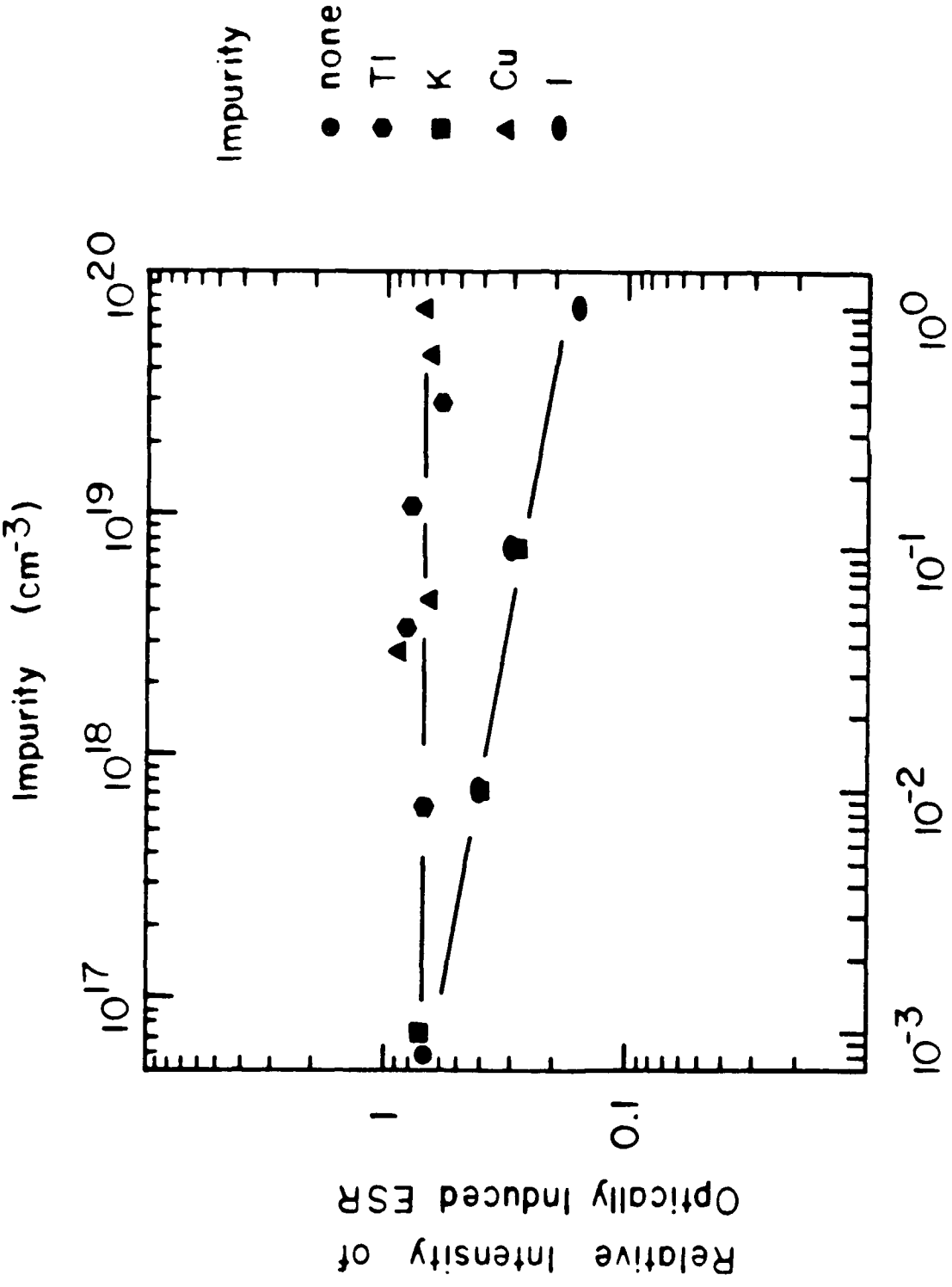
Impurity
none
Tl
K
Cu
I
Impurity (cm-3)
10^17
10^18
10^19
10^20
Atomic % Impurity
10^-3
10^-2
10^-1
10^0
Relative Intensity of
Optically Induced ESR
0.1
1

Fig. 8

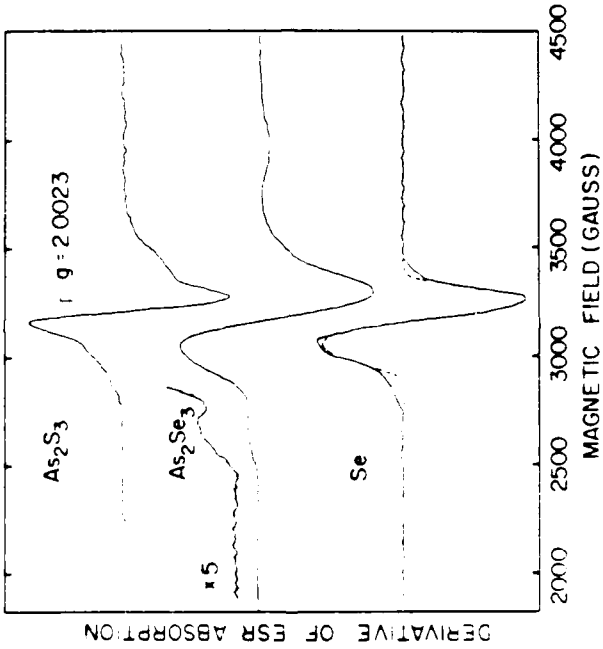
DERIVATIVE OF ESR ABSORPTION
2000
2500
3000
3500
4000
4500
MAGNETIC FIELD (GAUSS)
g = 2.0023
As2S3
As2Se3
Se
x5

Fig. 7

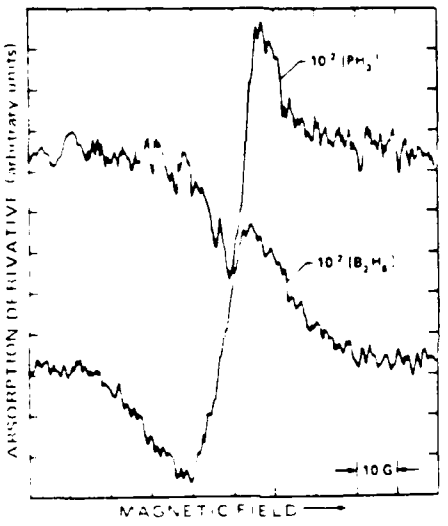

Fig. 6

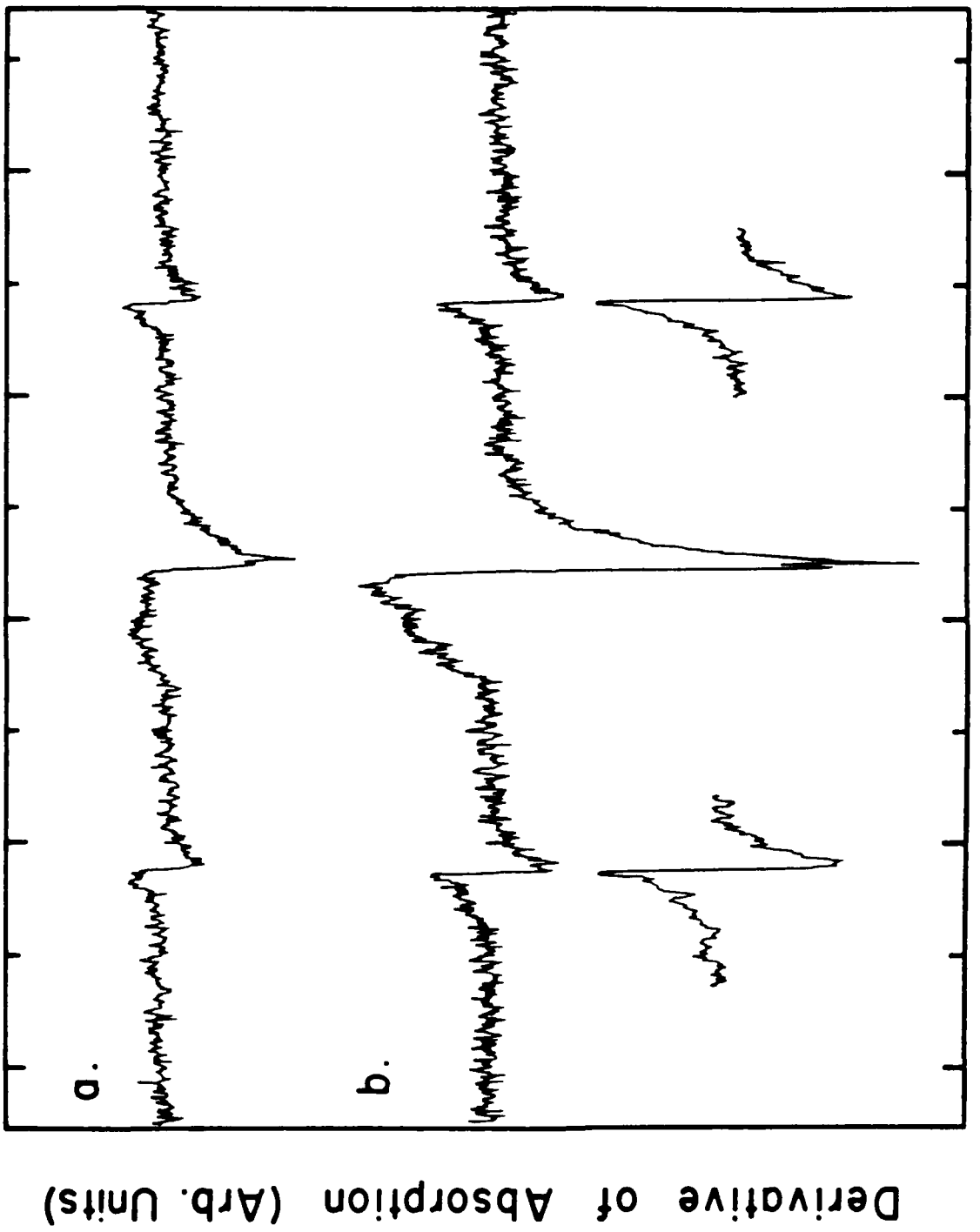
a.
b.
3000
3200
3400
3600
Magnetic Field (G)
Derivative of Absorption (Arb. Units)

Fig. 5

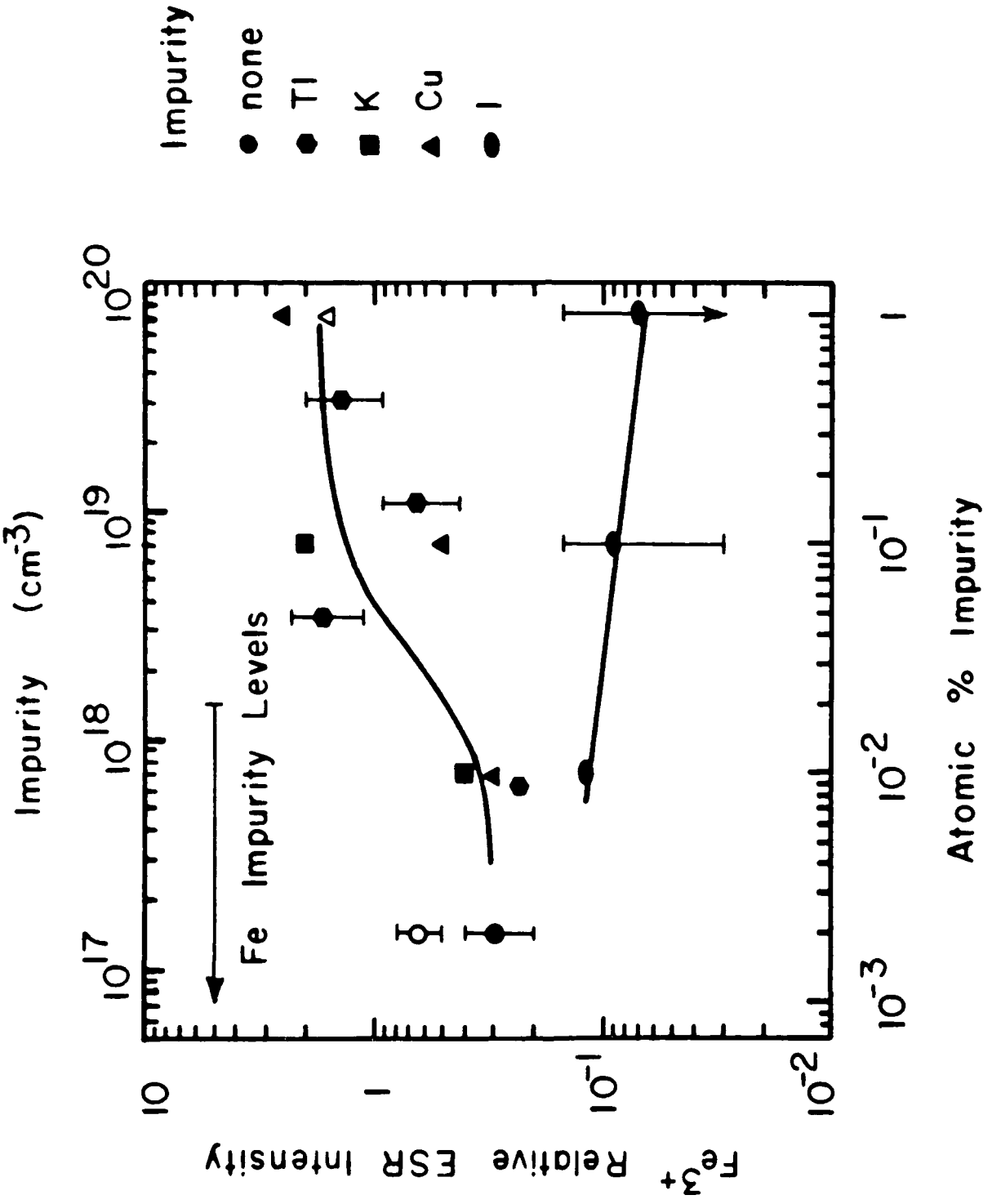
Impurity
none
Tl
K
Cu
I
Fe Impurity Levels
Impurity (cm-3)
Atomic % Impurity
Fe3+ Relative ESR Intensity

Fig. 4

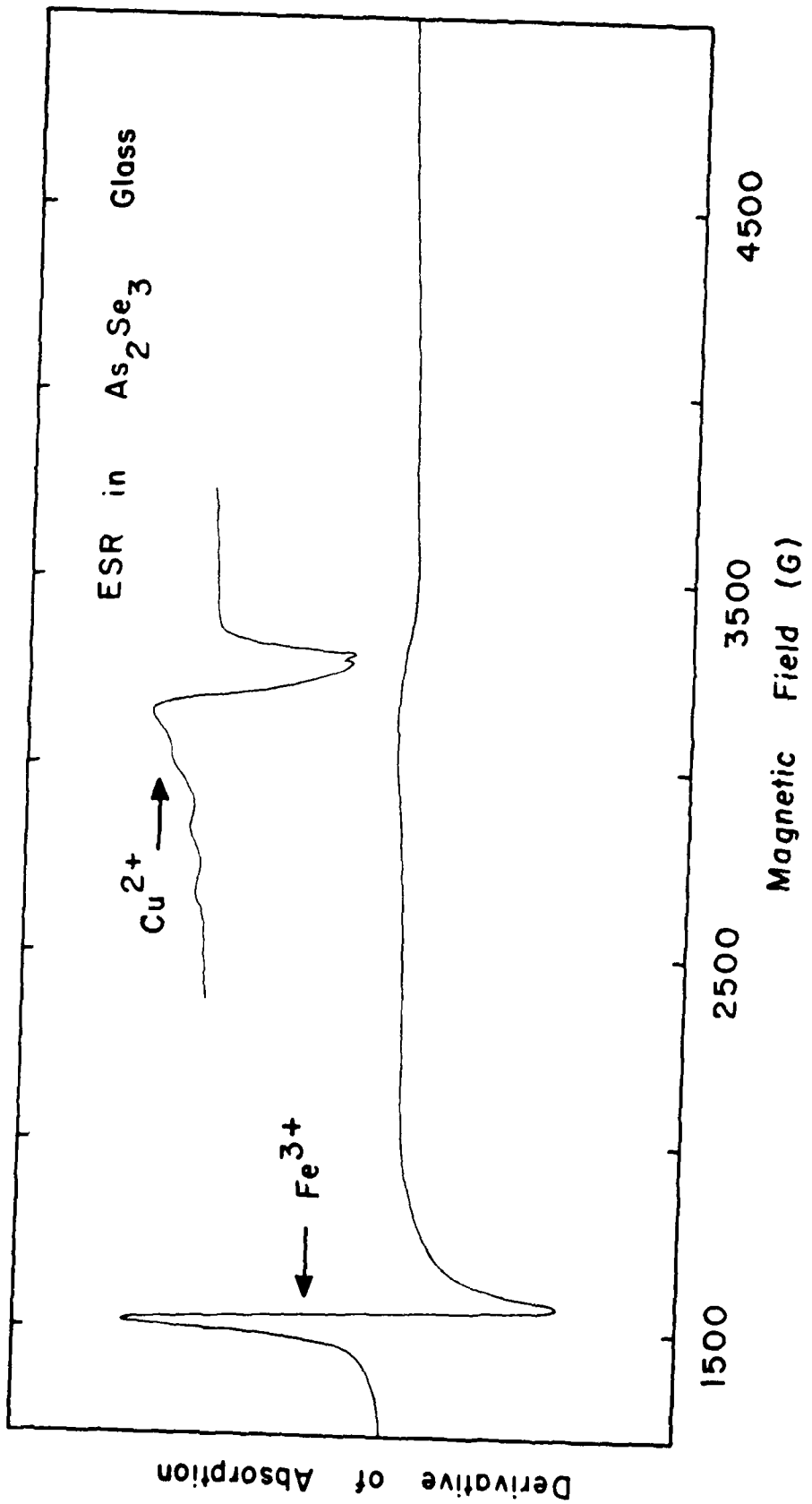
ESR in As_2Se_3 Glass
Cu^{2+}
Fe^{3+}
1500
2500
3500
4500
Magnetic Field (G)
Derivative of Absorption

Fig. 3

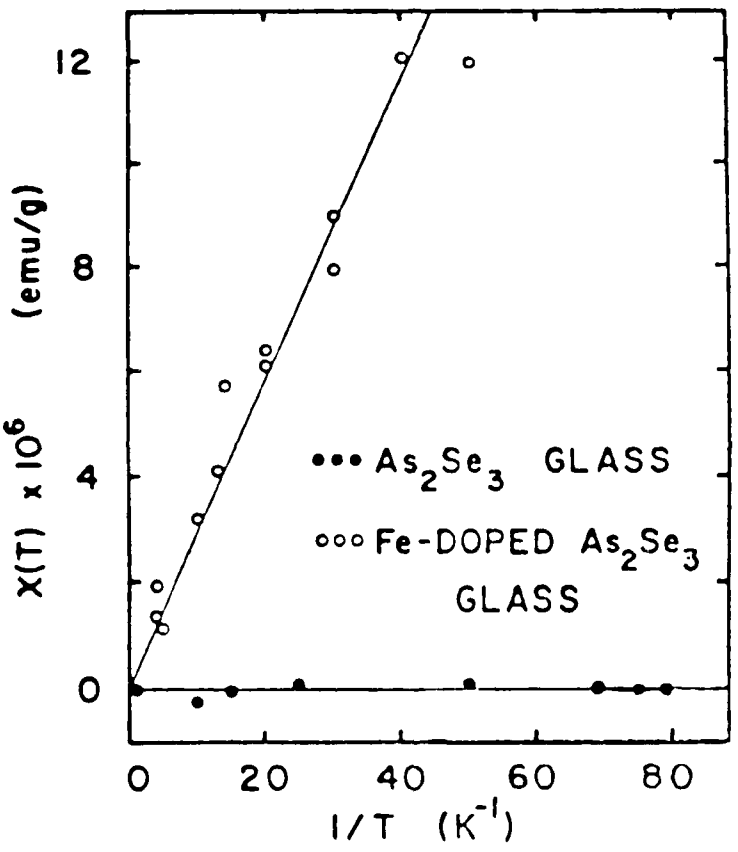
12
8
4
0
X(T) x 10^6 (emu/g)
••• As2Se3 GLASS
ooo Fe-DOPED As2Se3 GLASS
0
20
40
60
80
1/T (K^-1)

Fig. 2

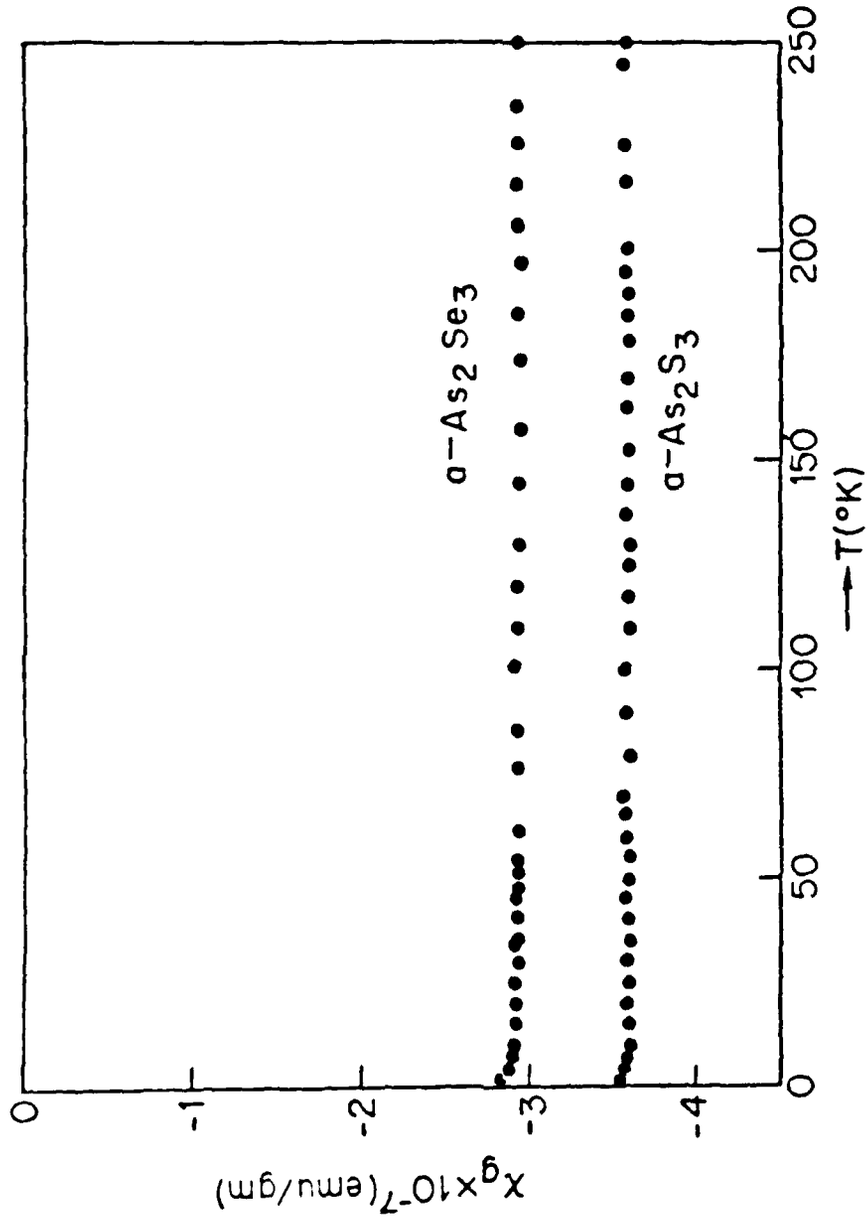

Fig. 1

Fig. 26. Change in value of T_1 at the minimum (~ 30K) as a function of the time held at 4.2K (inset) and the return of the value of T_1 at the minimum as a function of time t_a annealed at room temperature. (After ref. 112.)

freshly prepared sample stored at 77K for 2 days and three months, respectively. These data illustrate the lack of devitrification when the sample is stored at 77K. The triangles represent data taken on a second sample to illustrate reproducibility. The arrows at the top of the figure indicate the NQR frequency in claudetite I and arsenolite. See text for details.

Fig. 21. (a) NQR absorption in amorphous As (circles and solid line) and orthorhombic As (dashed line) at 4.2K. (b) Calculated contribution to NQR line shape from bonding electrons on nearest-neighbor atoms as described in the text. (The points refer to a calculated histrogram through which a smooth curve has been drawn.) Inset: dihedral angle distribution form Ref. 123. (After ref. 121.)

Fig. 22. ^{1}H NMR free induction decay in a-Si:H at 4.2 K (semilogarithmic scale). Circles represent experimental data. Inset: transformed frequency spectrum (linear scale). (After ref. 126.)

Fig. 23. Fourier transformed ^{11}B NMR spin-echo signal at 61 MHz in a-Si:H,B with approximately 10 at.% boron.

Fig. 24. Temperature dependence of T_1 for ^{75}As NQR in several amorphous semiconductors. Circles and squares represent data for amorphous As and glassy As_2S_3, respectively. The dashed line indicates the behavior in glassy As_2Se_3.

Fig. 25. T_1 as a function of temperature for a typical glow-discharge film of a-Si:H (circles) and a sputtered film of a-Si:H which was intentionally made with low hydrogen content (triangles). See text for details. (After ref. 147.)

Fig. 14. ESR spectra at x-band in amorphous As at ~ 10K. (After ref. 93.)

Fig. 15. Derivative of the ESR absorption as a function of magnetic field for (a) the center P_2 and (b) the center P_1 as described in the text. The solid curves represent computer simulations. The experimental curve in (a) is the difference between the x-irradiated spectra at 95 and 77K. The experimental curve in (b) is the difference between the x-irradiated and the unirradiated ESR spectrum above ~ 250K. (After ref. 95.)

Fig. 16. ESR spectra of a-Si:H at 30K and ~ 9 GHz. The optical excitation which produced these traces is 100 mW/cm^2 at 1.915 eV. Samples which are undoped and heavily boron- and phosphorus-doped are shown. (After ref. 100.)

Fig. 17. The ^{77}Se NMR spectra observed in glassy, molten and trigonal crystalline Se. The vertical line at 10 kG indicates the position of the ^{77}Se NMR in a standard sample (H_2SeO_3) at a frequency of 8.131 MHz. (After ref. 113.)

Fig. 18. Magnitude of the ^{205}Tl NMR isotropic chemical shift (relative to a 2.5 M solution of thallium acetate in water) in Tl-As-Se glasses as a function of Tl_2Se content. (After ref. 115.)

Fig. 19. Relative ^{75}As NQR echo intensity as a function of frequency at 77K in bulk, glassy As_2Se_3: Solid triangles represent data taken before irradiation and open circles represent data taken after irradiation at 77K with 6764 Å light. Solid lines and dashed lines at the top of the figure represent NQR frequencies of crystalline As_2Se_3 and crystalline As_4Se_4, respectively. (After ref. 117.)

Fig. 20. Relative ^{75}As NQR echo intensity as a function of frequency at 77K in glassy As_2O_3. Solid and open circles represent data taken on a

Fig. 8. Optically induced ESR intensity in Tl, Cu, K and I doped As_2Se_3 glasses as a function of dopant concentration.

Fig. 9. Optically-induced ESR spectrum near 4.2K in glassy As_2Se_3 doped with 0.9 at.% I. The dashed curve is the As-related center described in the next section.

Fig. 10. X-band (9.210 GHz) ESR spectra near 4.2K of (a) pure As_2S_3 and (b) As_2S_3+120 ppm Fe. The derivative features near 1500 G are due to Fe^{3+} and are essentially insensitive to the application of near-band gap light. The features near 3200 G are optically induced signals from which a "dark" background signal has been subtracted. (After ref. 31.)

Fig. 11. Derivative of ESR absorption as a function of magnetic field in x-irradiated As_2O_3 at 110K. (a) Experimental trace; (b) computer simulated spectrum for a Gaussian distribution of bonding hybridizations, and (c) computer simulation for a single site (with no s-p hybridization). (After ref. 84.)

Fig. 12. ESR derivative spectra (9.213 GHz) observed at 4.2K after x-irradiation at 77K in (a) GeS_2, (b) $GeSe_2$ and (c) As_2S_3 glasses. In (a) the lineshape is somewhat saturated by excessive microwave power. In (c) the narrow feature at g = 2.002 is distorted due to the large amplitude of the magnetic field modulation which was employed to enhance the broader features. (After ref. 33.)

Fig. 13. ESR spectra at x-band in glassy As_2S_3 and Ge_2S_8 at ~ 10K. The dashed lines are lineshapes attributed to the optical rearrangement of charge in existing defects and the solid lines to lineshapes attributed to the creation of new defects. Note in general the better resolution of the lines attributed to new defects. (After ref. 91.)

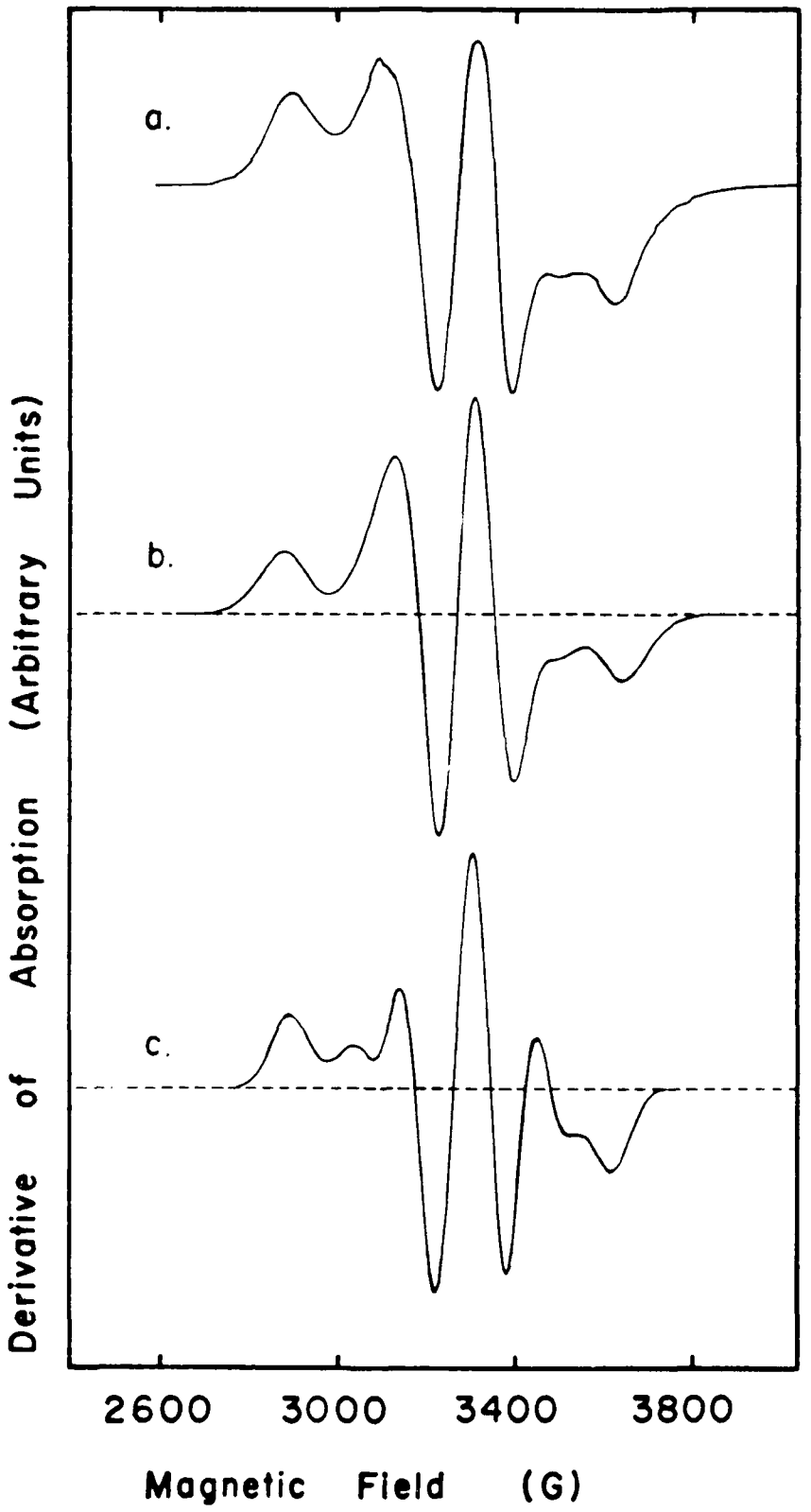
a.
b.
c.
Derivative of Absorption (Arbitrary Units)
2600
3000
3400
3800
Magnetic Field (G)

Fig. 11

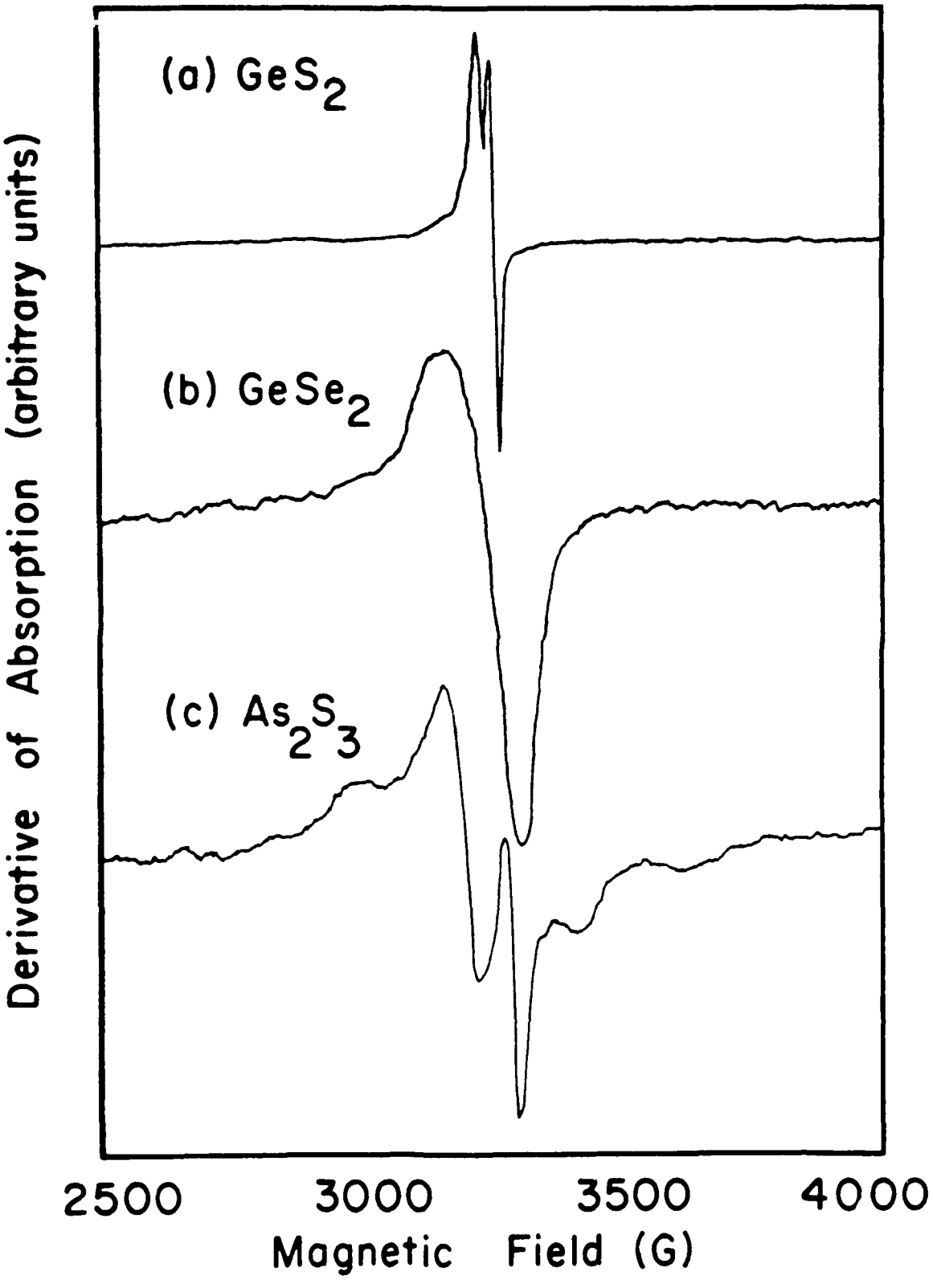
(a) GeS2
(b) GeSe2
(c) As2S3
Derivative of Absorption (arbitrary units)
2500
3000
3500
4000
Magnetic Field (G)

Fig. 1

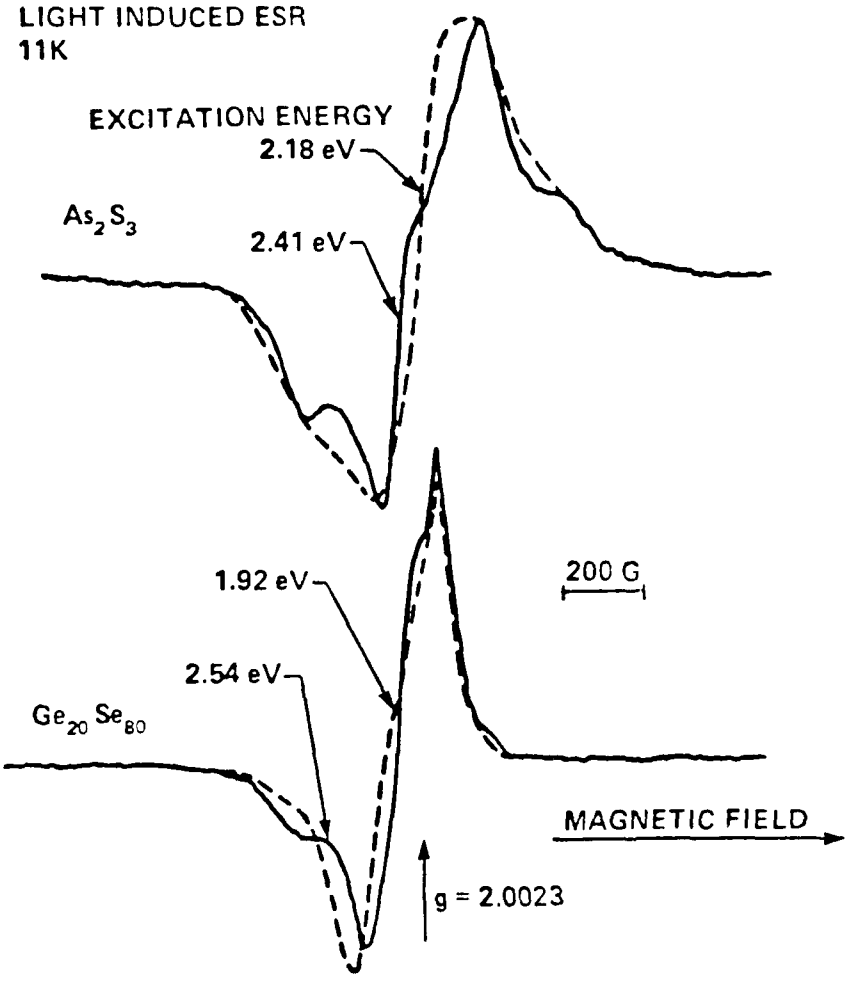
LIGHT INDUCED ESR
11K
EXCITATION ENERGY
2.18 eV
As2S3
2.41 eV
200 G
1.92 eV
2.54 eV
Ge20Se80
MAGNETIC FIELD
g = 2.0023

Fig. 12

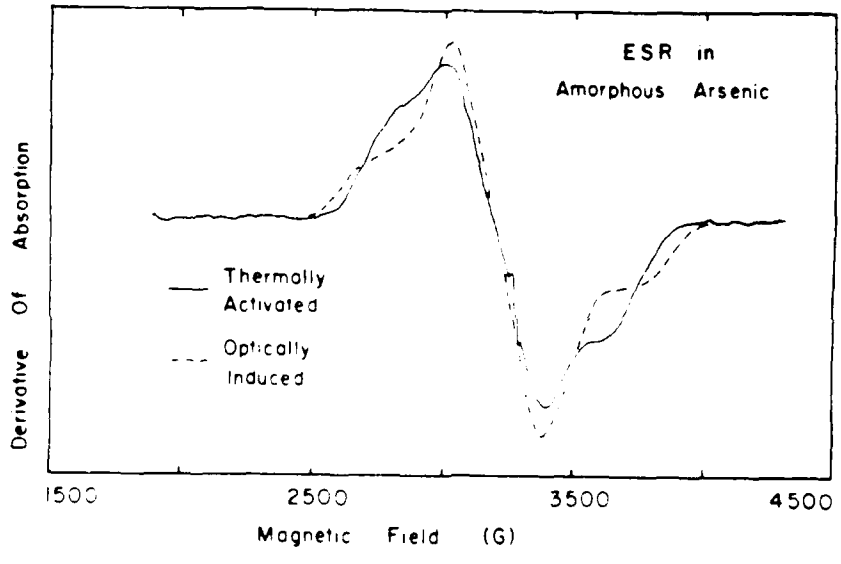
ESR in
Amorphous Arsenic
Thermally
Activated
Optically
Induced
Derivative Of Absorption
1500
2500
3500
4500
Magnetic Field (G)

Fig. 14

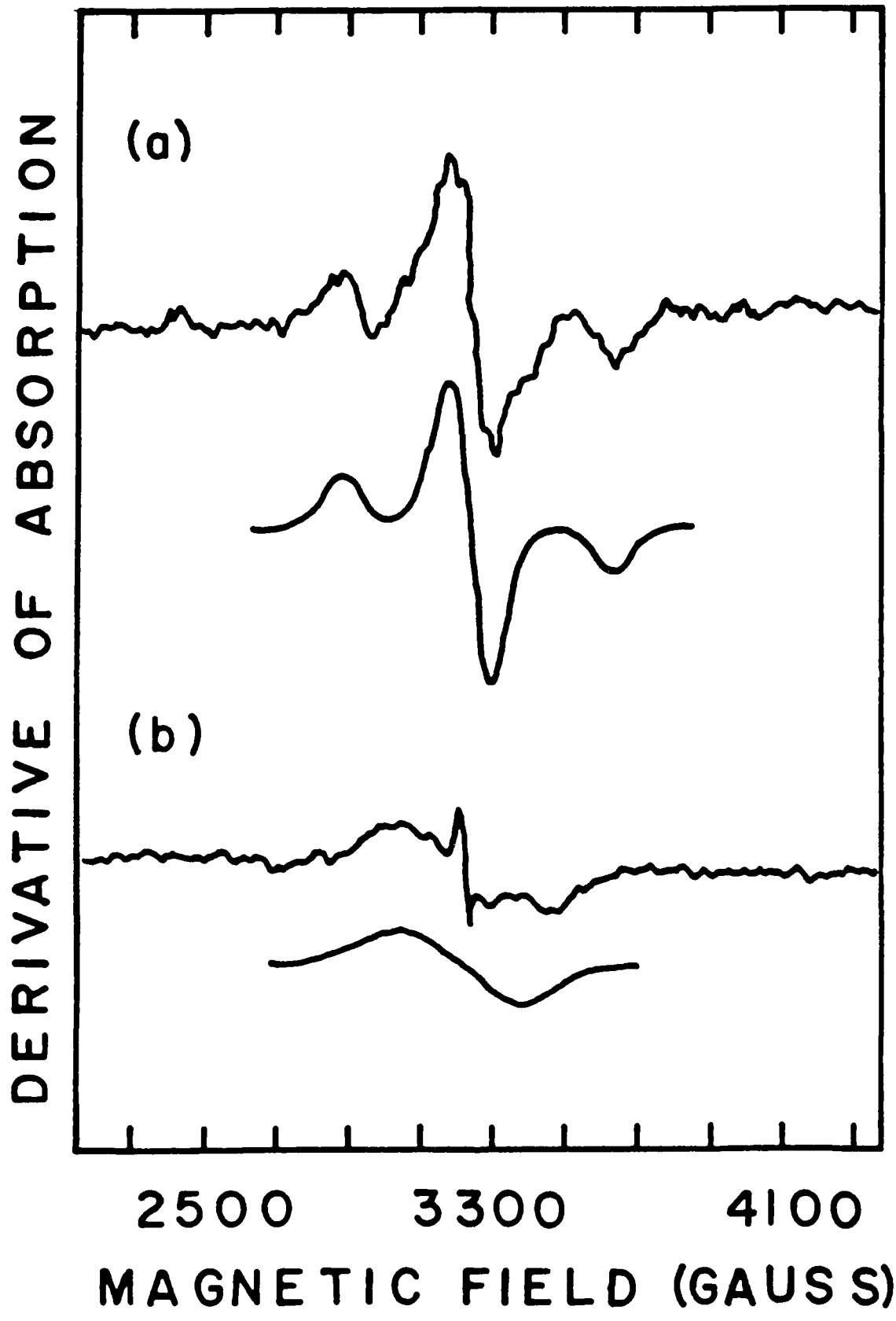
(a)
(b)
DERIVATIVE OF ABSORPTION
2500
3300
4100
MAGNETIC FIELD (GAUSS)

Fig. 15

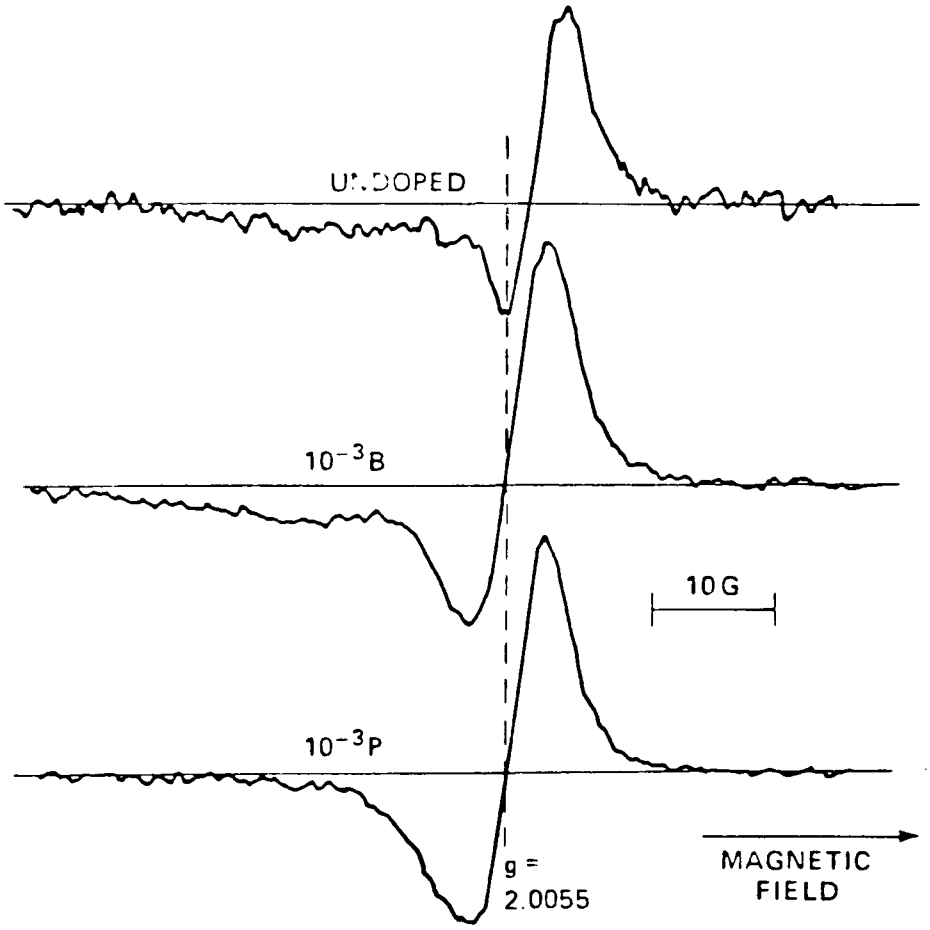

Fig. 16

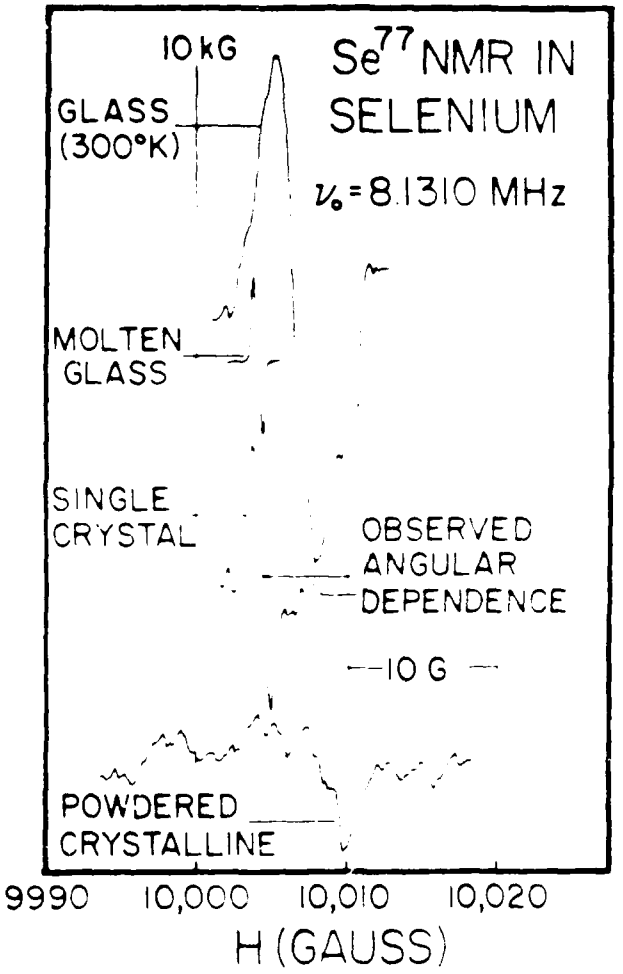
10 kG
Se77 NMR IN SELENIUM
GLASS (300°K)
ν0 = 8.1310 MHz
MOLTEN GLASS
SINGLE CRYSTAL
OBSERVED ANGULAR DEPENDENCE
10 G
POWDERED CRYSTALLINE
9990
10,000
10,010
10,020
H (GAUSS)

Fig. 17

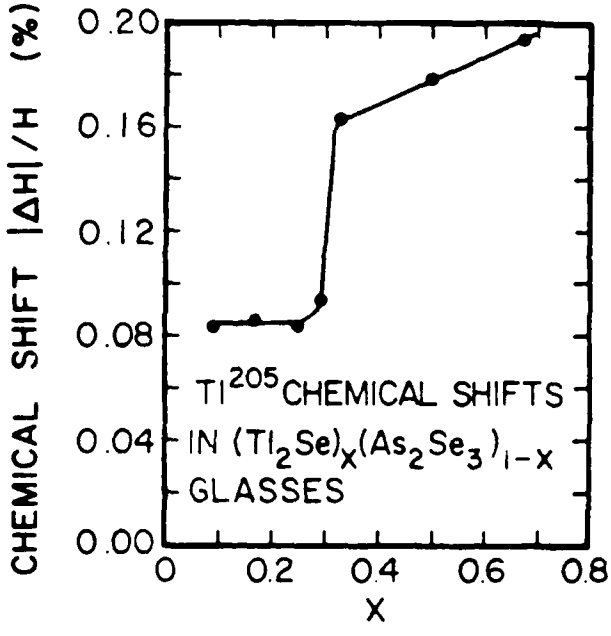
CHEMICAL SHIFT |ΔH|/H (%)
0.20
0.16
0.12
0.08
0.04
0.00
0
0.2
0.4
0.6
0.8
X
TI205 CHEMICAL SHIFTS
IN (TI2Se)X(As2Se3)1-X
GLASSES

Fig. 18

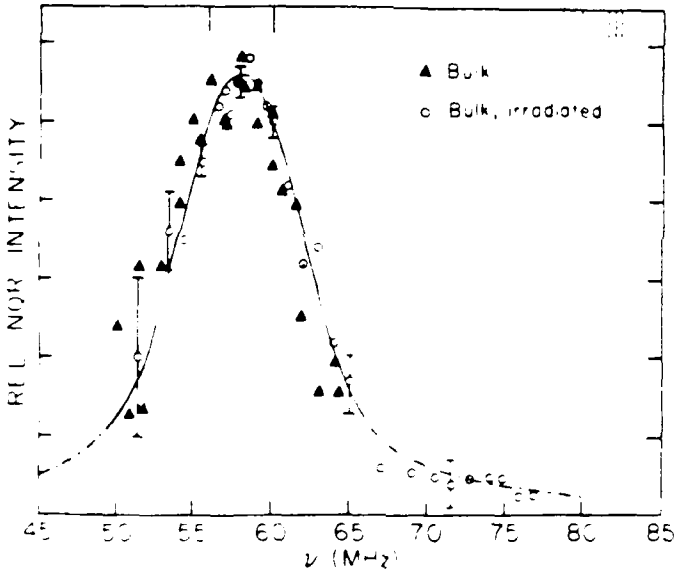
▲ Bulk
○ Bulk, irradiated
REL NOR INTENSITY
45
50
55
60
65
70
75
80
85
ν (MHz)

Fig. 19

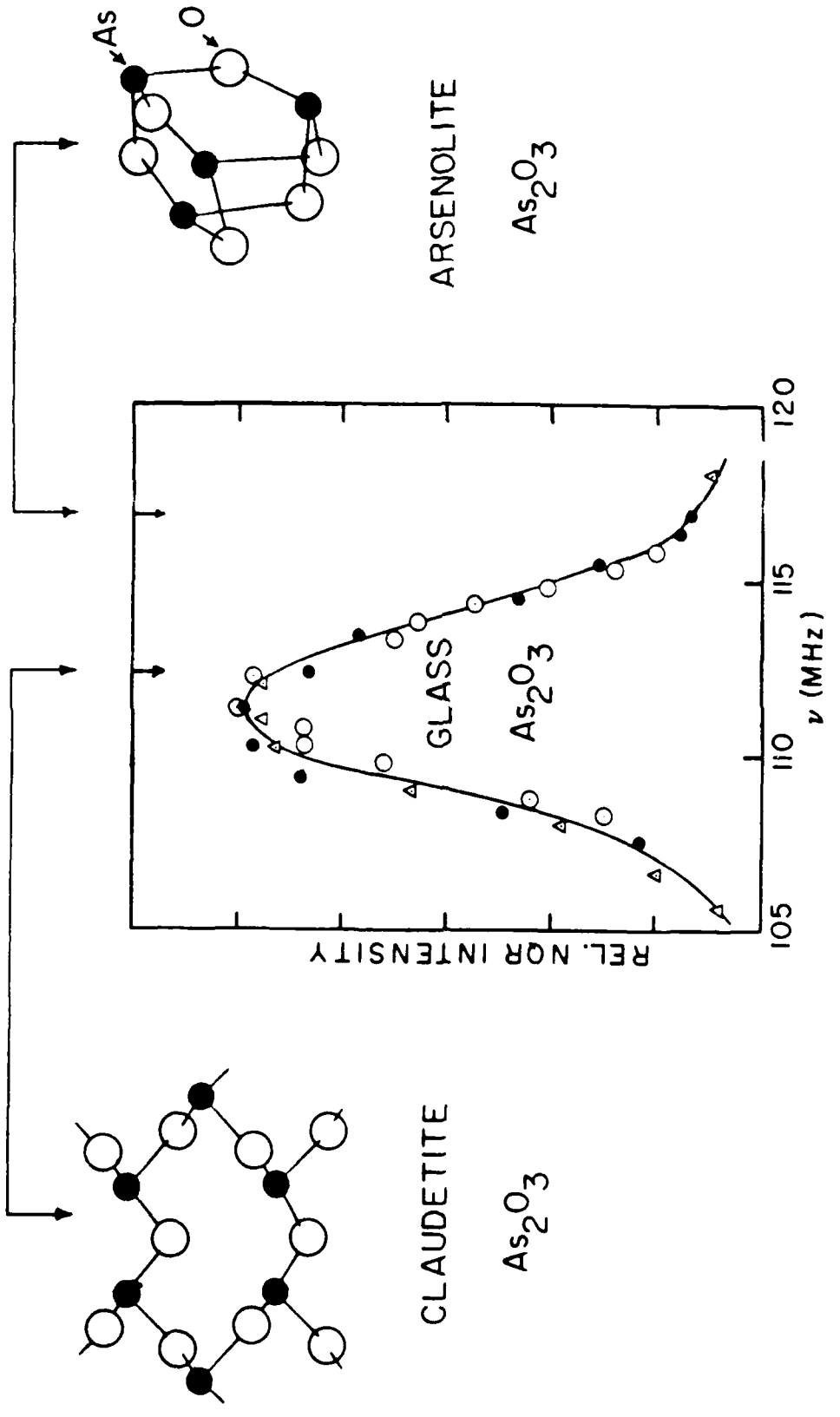
As
O
ARSENOLITE
As_2O_3
GLASS
As_2O_3
REL. NOR INTENSITY
105
110
115
120
ν (MHz)
CLAUDETITE
As_2O_3

Fig. 20

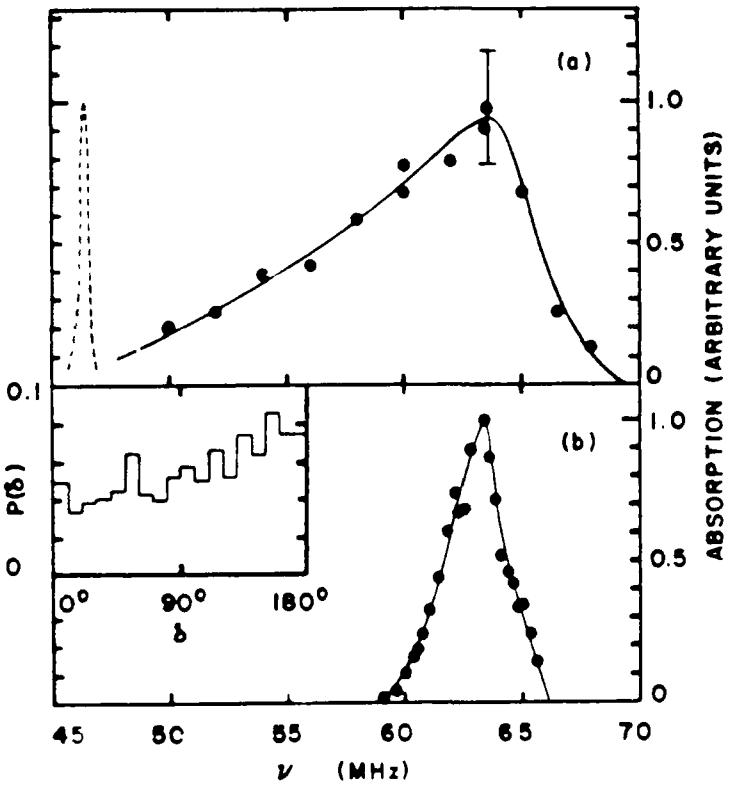
(a)
1.0
0.5
0
0.1
P(δ)
0
(b)
1.0
0.5
0
ABSORPTION (ARBITRARY UNITS)
0°
90°
180°
δ
45
50
55
60
65
70
ν (MHz)

Fig. 21

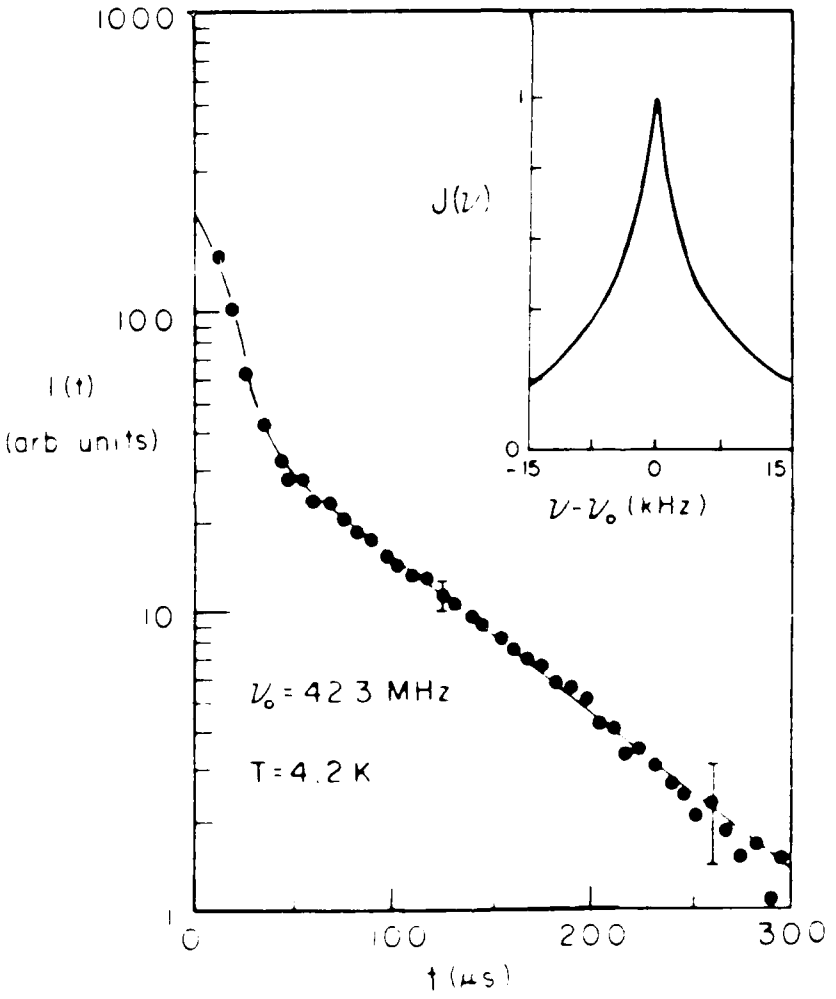
1000
100
10
1
I(t)
(arb units)
0
100
200
300
t (μs)
ν₀ = 42 3 MHz
T = 4.2 K
J(ν)
1
0
-15
0
15
ν-ν₀ (kHz)

Fig. 22

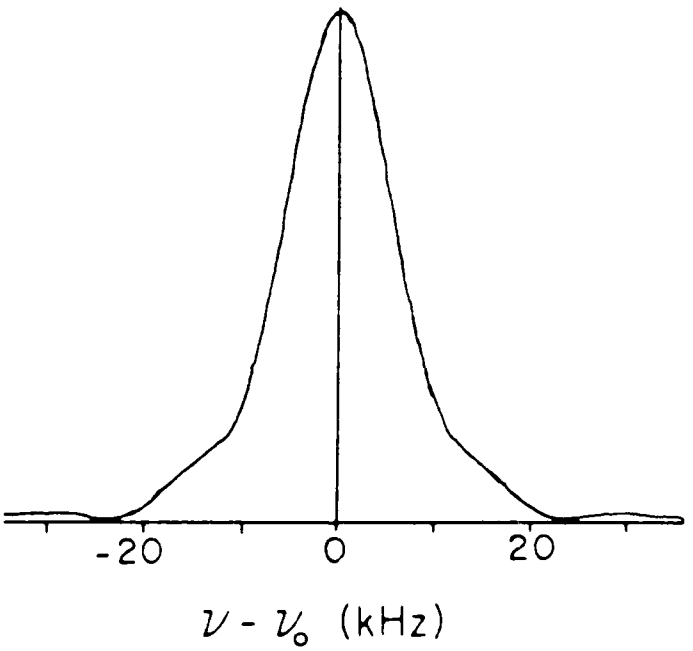

Fig. 23

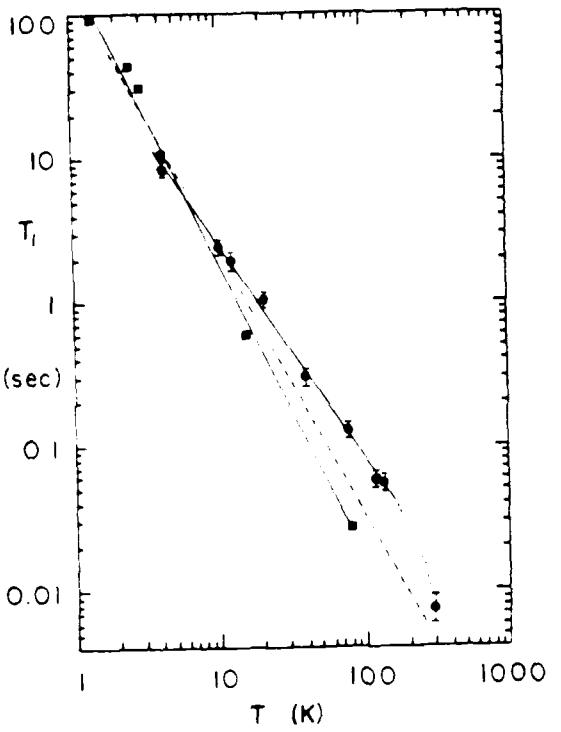

Fig. 9c

AD-A155 210 MAGNETIC EFFECTS IN NON-CRYSTALLINE SEMICONDUCTORS(U) 2/2
UTAH UNIV SALT LAKE CITY DEPT OF PHYSICS P C TAYLOR
1983 N00014-83-K-0535

UNCLASSIFIED F/G 20/12 NL

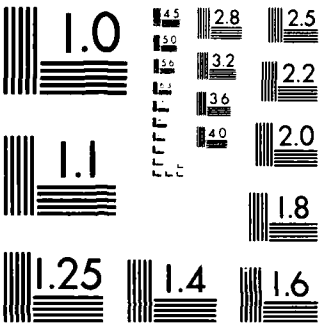

MICROCOPY RESOLUTION TEST CHART
NATIONAL BUREAU OF STANDARDS 1963 A

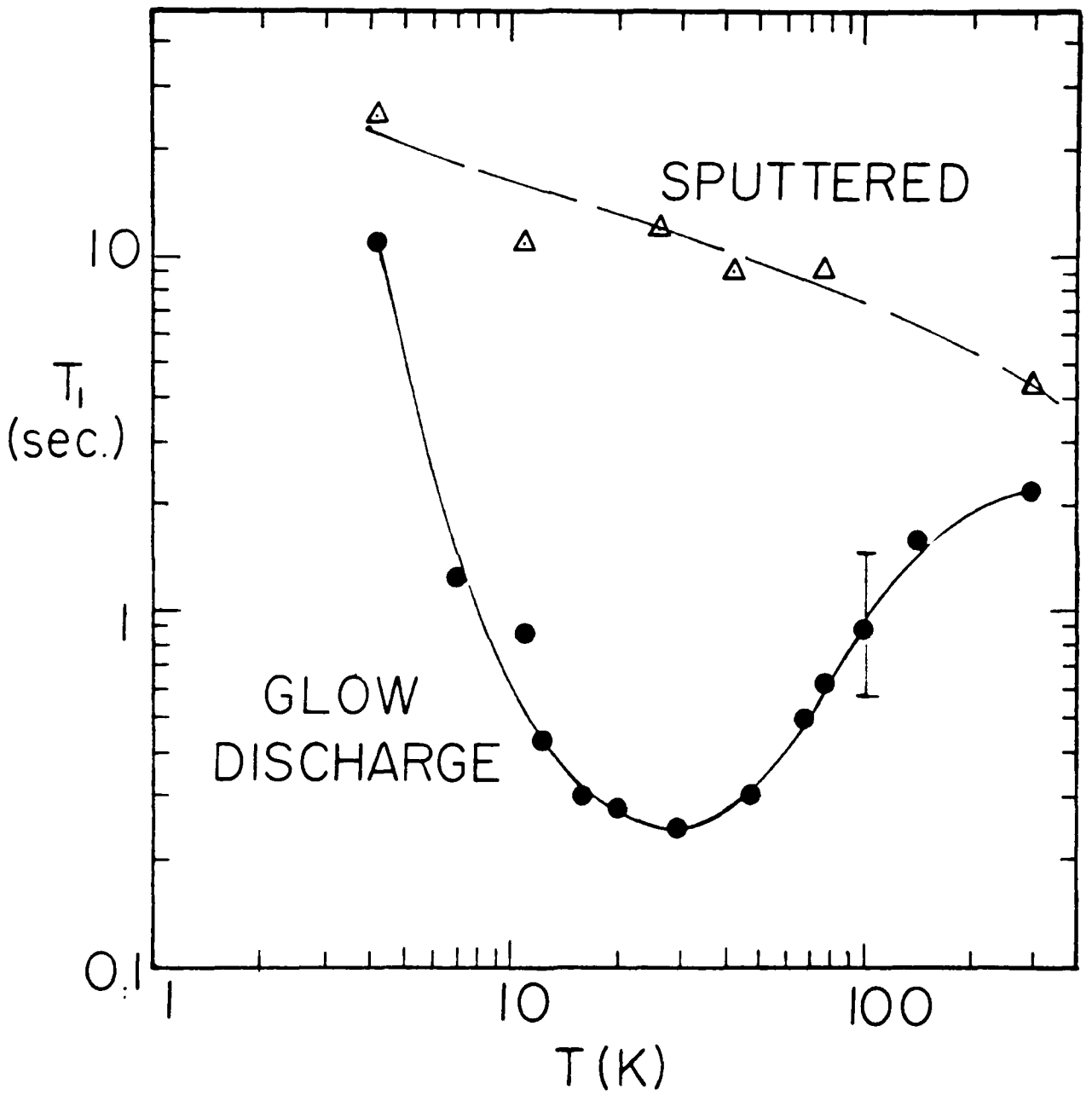

Fig. 25

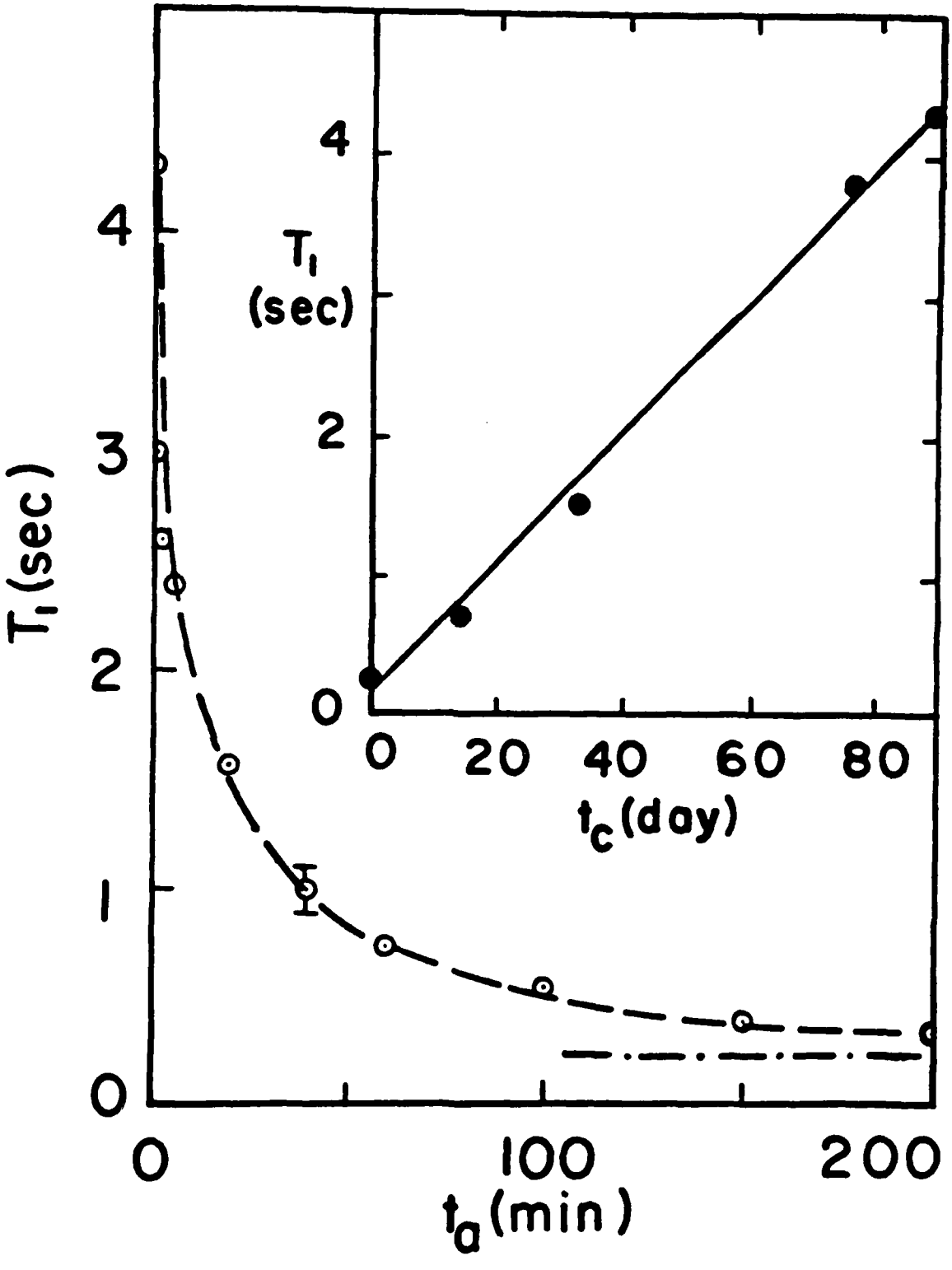

Fig. 26

END

FILMED

7-85

DTIC